Materials Advances

ROYAL SOCIETY OF CHEMISTRY

REVIEW

View Article Online
View Journal | View Issue

Cite this: *Mater. Adv.*, 2023, 4, 2885

Scalable production of microscopic particles for biological delivery

Huoyue Lin,†[a] Jing Leng,†[b] Pingqing Fan,[b] Zixing Xu*[abc] and Gang Ruan*[abcdef]

Received 12th January 2023,
Accepted 12th June 2023

DOI: 10.1039/d3ma00021d

rsc.li/materials-advances

Microscopic particles (nano- and micro-particles) have shown great potential as biological delivery carriers, with notable success stories such as in DOXIL and COVID-19 vaccines. Translation of these advanced drug delivery systems to industry/clinic is challenging, with scalable production being one of the keys. This review summarizes efforts in the literature in developing scalable production processes for microscopic particle-based bio-delivery systems. These scalable production processes include both batch processes and continuous processes such as microfluidics, flash technology, and electrospray. The materials used for particle-based delivery carriers include organic, inorganic, as well as hybrid materials. Finally, we also discuss the downstream processes after production, *e.g.*, purification, bioconjugation, sterilization, and storage.

1. Introduction

Biological delivery is the delivery of cargos (*e.g.*, drugs, nucleic acids, proteins, and imaging agents) in biological systems. It is recognized as one of the most important problems to solve in biotechnology and bioengineering.[1,2] The field of biological delivery has its origins in pharmacy's 'drug formulation'. Conventional drug formulation has many limitations. For example, formulating a siRNA drug in a conventional tablet does little to protect the siRNA from being degraded by nucleases in the physiological environment. Commercial introduction of microscopic particles (nano- or micro- particles, size range 1 nm to 500 μm) as biological delivery systems started with Lepron Depot® (in 1989) and Doxil® (in 1995).[3,4] Lepron Depot® is a polymer microparticle injectable formulation of gonadotropin-releasing hormone, and Doxil® is a PEGylated liposome formulation of doxorubicin. Microscopic particle-based delivery systems are often called 'advanced drug delivery systems', as they can offer the abilities of sustained drug release, stimuli-triggered drug release, timed delivery of multiple drugs, cargo protection, targeting, *etc.* Since the 2000s, inorganic nanoparticles (*e.g.*, iron oxide, quantum dots, gold, and silica) started to be introduced in the biological delivery field.[5–10] In addition to delivery, many inorganic nanoparticles can also

[a] *Department of Biomedical Engineering, College of Engineering and Applied Sciences, Nanjing University, Nanjing, 210093, China. E-mail: Gang.Ruan@xjtlu.edu.cn, 1069690400@qq.com*
[b] *Wisdom Lake Academy of Pharmacy, Xi'an Jiaotong-Liverpool University, Suzhou, 215123, China*
[c] *Nanobiotechnology & Nanomedicine Center, Xi'an Jiaotong-Liverpool University, Suzhou, 215123, China*
[d] *Cell & Gene Therapy Center, Xi'an Jiaotong-Liverpool University, Suzhou, 215123, China*
[e] *Institute of Materials Engineering of Nanjing University, Nantong, 210033, China*
[f] *Shenzhen Research Institute of Nanjing University, Shenzhen, 518063, China*
† These authors contributed equally.

Huoyue Lin

Huoyue Lin graduated from the College of Textiles at Donghua University (China) in 2020. She then received her Master's Degree at the College of Engineering and Applied Sciences at Nanjing University (China) in 2023, working under the supervision of Prof. Gang Ruan. Her research interests include self-assembly and biological delivery.

Jing Leng

Jing Leng received her bachelor and master degrees in materials science from Harbin Science & Technology University (China). She currently works as a technician in the research group of Prof. Gang Ruan.

offer the abilities of imaging or/and physics-based therapies (therapies based on heat, light, *etc.*), due to their special quantum mechanics-based physical properties.[5–10] Most recently, the global pandemic of COVID-19 has seen by far the greatest societal impact of microscopic particle-based delivery, as mRNA vaccines with lipid nanoparticles (LNPs) as the delivery carriers were distributed to billions of people worldwide.[11] Thus, it is now clear that microscopic particle-based delivery represents a trend in biological delivery. This is especially true for newer therapeutics such as siRNAs, mRNAs and proteins, due to their bulky sizes and fragile structures.

For a new microscopic particle-based delivery system to enter the clinic, a proof-of-concept study to demonstrate its functionalities is only the beginning. A number of further technical hurdles need to be addressed, such as production, toxicology, *etc.* This review focuses on the production issue. Translating a laboratory invention of pharmaceuticals to industry requires industrial implementation of processes in which chemical, physical, or microbiological conversion of materials takes place in conjunction with the transfer of mass, heat, and momentum. The transport phenomena (mass transfer, heat transfer, and momentum transfer) are scale dependent; that is, they behave differently on a small scale (laboratory production scale typical range being 10–1000 mg) and on a large scale (commercial production scale typically being 100–1000 times of the laboratory scale). A scalable production process needs to have the ability to reasonably easily accommodate changes in scales (here primarily referring to an increase in scale, that is, scale up). Using microscopic particles as the delivery systems brings extra challenges into production, due to the inherent structural complexity of these systems. One needs to precisely control a number of structural parameters, *e.g.*, particle size, size distribution, surface morphology, surface chemistry, porosity, pore size distribution, pore connectivity, drug loading amount, and drug's spatial distribution in the particles, in a reproducible manner. Furthermore, this control needs to be achieved not only for lab-scale production, but industrial production. From a chemical engineering point of view, it is challenging to maintain the same Damköhler number (Da), the ratio between the reaction rate and transport phenomena rate, across different scales (from the smaller device volume in the lab scale to the larger device volume in the industrial scale). In addition, the required reproducibility for industrial production is usually much higher than lab-scale production. Two notable examples of production-caused disturbance to commercial microscopic particle-based delivery systems are: (1) temporary stoppage of production of Doxil® by Ben Venue Laboratories in 2011–2013, citing quality control deficiencies as the reason for production stoppage, causing a global shortage of Doxil® supply;[12] (2) discontinuation of Nutropin Depot® (polymer particle-based, long-acting form of human growth hormone) by Genetech in 2004, citing the significant resources needed for manufacturing the products as a main reason behind the decision.[13] Although more details about the exact reasons behind the disturbances are unavailable in the public domain in these two examples, it is clear that it was commercial manufacturing challenges that caused the disturbances. In principle, to scale up a production process of

Pingqing Fan

Pingqing Fan received her bachelor degree in 2018 from Monash University (Australia), majoring in chemistry with a minor in genetics. She received her master degree from Leeds University (UK) in 2020, majoring in polymer chemistry. She then worked in WuXi AppTec as a research engineer. She is now a PhD student in Prof. Gang Ruan's group developing gene delivery technologies.

Zixing Xu

Zixing Xu received her bachelor degree in biomedical engineering in 2019 from Nanjing University (China). She is currently a senior PhD student in Prof. Gang Ruan's group. Her research interests include nano-biomaterials, drug delivery, and neural technologies.

Gang Ruan

Gang Ruan received his PhD from the National University of Singapore. He then worked in the US, first as a postdoctoral researcher then as a research scientist, in Emory University and the Ohio State University. He then moved to China, taking a faculty position in Nanjing University in 2013, and most recently in Xi'an Jiaotong-Liverpool University in 2022. His research interests include biological delivery and bio-imaging, regenerative medicine and neural medicine technologies, and nanobiomaterials. In addition to academic research, he co-founded Core Quantum Technologies Inc., translating nanobiomaterials-based technologies to the marketplace.

microscopic particle-based delivery systems, one can adopt the same principles of process scale-up used in traditional chemical/pharmaceutical engineering, *e.g.*, dimensional analysis.[14,15] An important trend is that we are witnessing increasing efforts to employ continuous processes for producing microscopic particle-based delivery systems. This review will summarize the literature on efforts of scalable production of various types of microscopic particle-based delivery systems. In addition, this review will also touch upon downstream processes after production, namely purification, bioconjugation, sterilization, and storage.

2. Organic particle-based delivery systems

2.1 Lipid particle-based delivery systems

Multilamellar lipid structures were first discovered in 1964.[16] The lamellar (multi-lamellar or uni-lamellar) lipid vesicles (liposomes) were dubbed 'artificial cells'. Doxil® (anticancer drug doxorubicin-encapsulated liposomes) is one of the first commercial liposomal formulations, and is often cited as the face of early nanomedicine.[13] Since the regulatory approval of Doxil® more than a dozen lipid particle-based delivery systems have been in clinical use.[17,18] In addition to delivering small molecule drugs, lipid particles have been clinically successful in delivering nucleic acids. Onpattro® (siRNA in lipid nanoparticles) was approved in 2018 to treat polyneuropathies induced by hereditary transthyretin amyloidosis.[18] Most recently, Comiranty® and Spikevax® (mRNA in lipid nanoparticles) were approved in 2021 and 2022, respectively, as vaccines against COVID-19.[19]

Laboratory preparation of liposomes typically involves solvent evaporation (film hydration), solvent dispersion, or reverse phase evaporation, resulting in multi-lamellar vesicles (MLVs). This is often followed by a size reduction treatment by extrusion, sonication, or homogenization, yielding large uni-lamellar vesicles (LUVs) or small uni-lamellar vesicles (SUVs).[20] Other laboratory-scale methods for liposome preparation include thin-layer dispersion, reverse phase evaporation, ethanol injection, *etc.* These methods have a number of limitations as follows. It is worth mentioning that not all of these limitations are exactly about scale-up; some of them are inherent challenges related to specific production processes.

(i) These batch processes are difficult to perform at large scale maintaining a similar ratio of reaction rate to transport phenomena rate as the laboratory-scale process.

(ii) Batch-to-batch variations are often large. The thus-prepared liposomes are often heterogeneous. The sonication/extrusion treatments (used to reduce particle size and polydispersity) involve high energy and could result in degradation of drugs.

(iii) Many key instruments used are not readily available for industry-scale production.

(iv) The batch production involves many steps, including buffer preparation, phospholipid solution preparation, lipid hydration, extrusion, dilution, aseptic filtration, *etc.* The transitions between steps can be slow and inefficient.

(v) In a batch process, interactions between particles can be high, leading to aggregation.

Thus, an important component of technological innovation of liposomes and other lipid particle-based delivery systems has been developing their scalable production methods. Wangner *et al.* reported the crossflow injection technique operated at a pilot plant scale to produce liposomes encapsulating recombinant human superoxide dismutase (rh-Cu/Zn-SOD).[21] This technique was an advancement of the ethanol injection method. Ethanol injection is one of the most promising and high-energy free manufacturing methods to produce liposomes with required key qualities at large scale.[22] By injecting an ethanol solution containing lipids into a large volume of aqueous phase, phospholipid bilayer vesicles can be formed rapidly. Ethanol injection production is quite simple, rapid and safe. And it is applicable to different active pharmaceutical ingredients (APIs). In Wangner *et al.*'s method, the production plant was designed to prepare sterile liposomes without the need of sterilization of the end products. The core of the production system was the crossflow injection module, which was made of two stainless steel tubes welded together forming a cross. At the connecting point the module had an injection hole (250 μm drill hole). It was believed that the crossflow injection technique had the benefit of well-defined injection streams, thereby permitting liposome manufacture regardless of production scale, as scale was determined only by the free disposable vessel volume. Fig. 1 is a schematic illustration of the pilot plant. The protein solution was pumped from vessel A to vessel B passing the crossflow injection module, where the ethanol/lipid solution was injected into the protein solution, which was immediately diluted in the stirred buffer solution in vessel B. It was stated in this study that the manufacturing scale of several liters was feasible. Flow dynamics studies were performed in ref. 23 and 24, demonstrating that the crossflow injection indeed met the above-mentioned requirements.

Pham *et al.* described a membrane-based technique for producing liposomes at a pilot plant scale, which was also based on the principle of the ethanol injection process.[25] The core module for scalable production was a Shirasu porous glass (SPG) tubular membrane contactor. With the SPG membrane contactor, it was believed that scale-up was more straightforward, because the operation scaled linearly. As shown in Fig. 2, the membrane contactor set-up included a positive displacement pump, a pressurized vessel, equipped with a manometer M1, connected on one side to a nitrogen bottle and on the other side to the SPG membrane with two manometers (placed at the inlet and outlet of the module). The membrane system can regulate the size and size distribution of liposomes by adjusting the pore size of the membrane. The production scale can be controlled by adjusting the length of the membrane and manufacturing time. In this study, when a syringe-pump device was used for laboratory scale production, 30 mL per batch of liposomes were obtained; then when the SPG membrane contactor was used for pilot scale production, 750 mL per batch of liposomes was obtained.

Microfluidics-based production of lipid nanoparticles has become enormously successful thanks to the mRNA vaccines against COVID-19 manufactured by BioNTech/Pfizer and

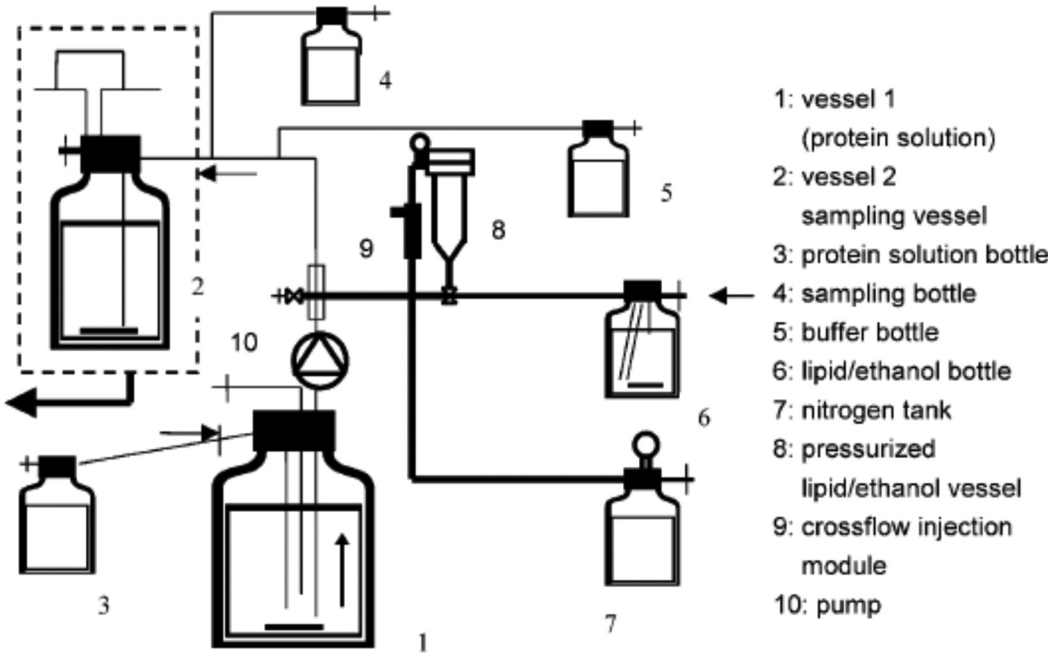

Fig. 1 Schematic of the pilot plant for production of protein-encapsulated liposomes by the crossflow injection technique. The protein solution is pumped from vessel 1 through the injection module, where liposomes are formed. The lipid/ethanol solution is injected with nitrogen pressure (vessel 7 nitrogen tank). Immediately after the injection procedure in the injection module the liposome suspension is diluted with buffer solution in vessel 2. This figure is adopted from ref. 21 with permission.

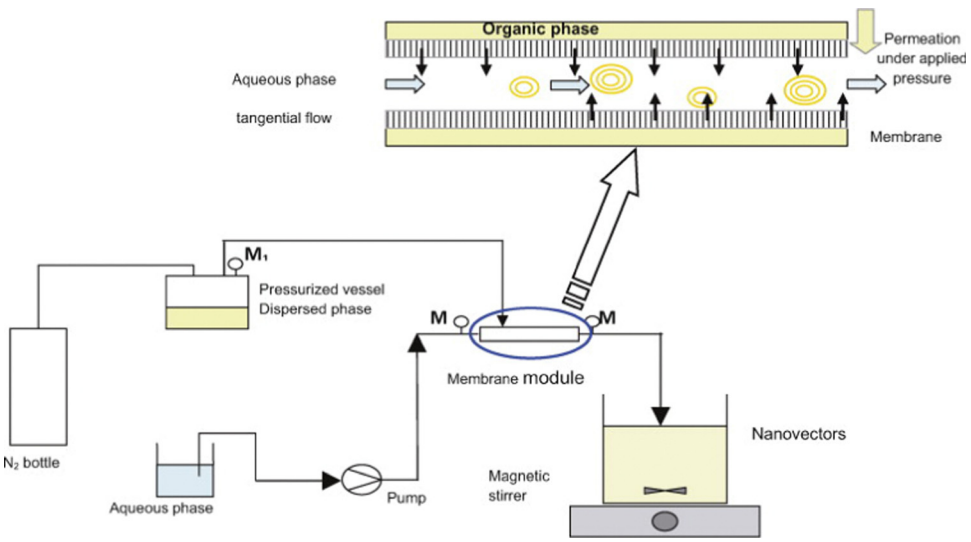

Fig. 2 Schematic drawing of the membrane contactor-based production set-up for liposomes. This figure is adopted from ref. 25 with permission.

Moderna/AstraZeneca (Comiranty® and Spikevax®, respectively). Compared to bulk methods, microfluidics offers many unique capabilities, making it ideal for scalable production of microscopic particles for drug delivery, such as: (1) fast mixing and rapid mass transfer, (2) precise control of process conditions, (3) low degree of aggregation, because nanoparticles move with flows, (4) reproducible product properties, (5) automatic sampler and software control are available to automate the system, (6) integrating on-line analysis is possible to improve the quality control of the production process, and (7) microfluidics can be readily scaled up by parallelization.[26–30] The above features of microfluidics have been validated in BioNTech/Pfizer and Moderna/AstraZeneca's manufacture of mRNA-loaded lipid nanoparticles as COVID-19 vaccines. The following is a brief summary of how Pfizer produces its millions of COVID-19 vaccine doses.[31] An impingement jet mixer (IJM) of a US quarter coin size, also known as the tea stirrer, is used. A lipid solution is mixed with an mRNA solution by pumping lipids from one channel and mRNA from the other,

forcing them to mix together with 400 pounds of pressure. To meet the requirement of large-scale production, instead of using a large mixer, Pfizer uses a parallelization of 100 quarter-sized mixers. This permits continuous synthesis of 100 million vaccine doses per month at the Kalamazoo (US) production site. A computer system is established to automate the manufacturing process. Fig. 3 shows photos of the IJM devices used in the laboratory and in industry for comparison.[32]

Two widely-used microfluidic designs are hydrodynamic flow focusing (HFF)[33–35] and staggered herringbone micromixer (Fig. 4a and b).[36–38] External fields, *e.g.*, acoustofluidics, can be employed to enhance mixing (Fig. 4c).[39,40] HFF utilizes the laminar regime typically found within microfluidic platforms. In HFF, a narrow stream of fluid, typically lipid, polymer, or other NP precursor dissolved in a solvent flows in parallel with an antisolvent (*e.g.*, water or buffer solution) from the two side channels (Fig. 4a). Due to the laminar flow regime present within the device, rapid mixing occurs through diffusion. Mixing time correlates with several parameters as follows:

$$t_{\mathrm{mix}} \sim \frac{w_{\mathrm{f}}^2}{4D} \approx \frac{w^2}{9D}\left[\frac{1}{\left(1+{}^1/_R\right)^2}\right]$$

where D is the diffusivity of the solvent, w_{f} is the width of the focused stream, w is the channel width, and R is the flow rate ratio of the middle stream to the flow rate of the sheath stream. Based on this equation, mixing time correlates positively with the width of the central stream, but negatively with the diffusivity of the solvent. As w_{f} is dependent on both the width of the channel and the flow rate ratio, a smaller channel with bigger flow rates benefits shorter mixing time, thus smaller particle size and better uniformity. Therefore, HFF allows for a greater degree of control over nanoparticle synthesis compared to conventional batch methods. Also, by designing HFF with different channel widths and tuning the flow rate ratio, it can be used to produce highly tunable nanoparticles with controlled size and size distribution.

The throughput of hydrodynamic flow focusing is usually very low. To overcome this limitation, turbulent flow is introduced to promote more rapid mixing. This is done by utilizing a new geometric design of mixer (*e.g.*, staggered herringbone micromixers, Fig. 4b), or/and employing an external energy source (*e.g.*, acoustic micromixing, Fig. 4c). A commercial microfluidic platform NanoAssemblr™ has been developed by Precision NanoSystems Inc. based on the staggered herringbone micromixing technology for lab scale and clinical scale microscopic particle manufacturing under GMP conditions.[41] The NanoAssemblr™ platform is a benchtop instrument integrating staggered herringbone microfluidic cartridges, syringe pumps, and computer software.

For microfluidics-based production, scaling up to the industry scale (with the common scale factor being 100–1000) has some inherent challenges.[42] Most of the key advantages of microfluidics-based production originates from its small channel size, giving rise to short transfer distances and high surface-to-volume ratios. However, scaling up 100–1000 times could require large increases of the channel dimensions, thereby diminishing the benefits of micro-channels. Parallelization (also called 'numbering up') could avoid this problem to a great extent. But parallelization often leads to significant challenges in fluid distribution, since a large number of channels is needed. In addition, for microfluidics-based production, and for continuous production in general, lag of regulatory guidelines is a significant impediment. Based on the advantages of continuous production, many organizations have expressed their support. The Center for Drug Evaluation and Research (CDER) of the FDA produced a draft guidance (Quality considerations for continuous manufacturing) in 2019. Recently, the International Coordinating Committee (ICH) adopted Q13 guidelines on continuous manufacturing of drug substances and drug products.

2.2 Polymer particle-based delivery systems

Microscopic particles made of synthetic or natural polymers have been used clinically for drug delivery for more than 30 years. Examples of synthetic polymers used include Poly(lactide) (PLA),

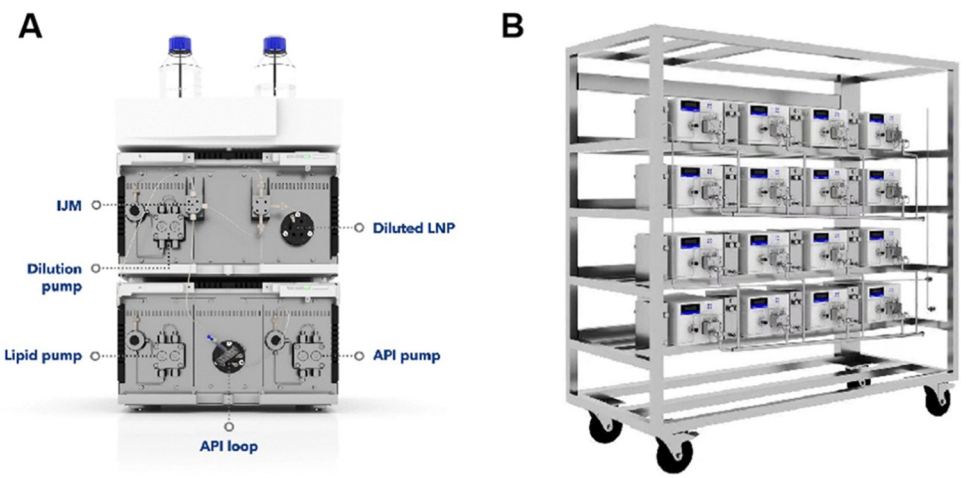

Fig. 3 IJM devices used in the laboratory (A) and industry (B). This figure is adopted from ref. 32 with permission.

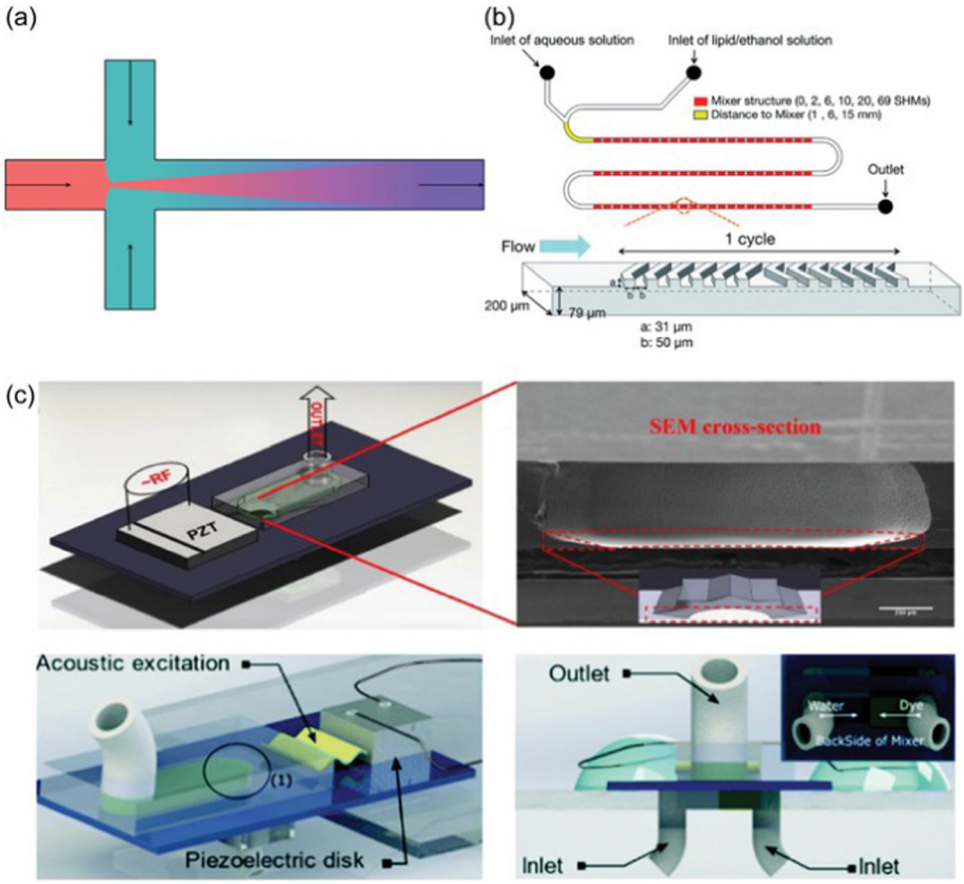

Fig. 4 Different microfluidic methods. (a) Schematic of hydrodynamic flow focusing. (b) Schematic of staggered herringbone micromixer. (c) Acoustic micromixing devices using star-shaped oscillating plates: the assembled star-shaped microfluidic mixer (top) and the ultrafast star-shaped acoustic micromixer (bottom). The figure is adopted from ref. 39 with permission.

poly(glycolide) (PGA), poly(lactide-*co*-glycolide) (PLGA), poly(cyanoacrylate) (PCA), polyethylenimine (PEI), and polycaprolactone (PCL). Examples of natural polymers used include chitosan, dextran, albumin, gelatin, alginate, and agar. The most commonly used polymer is PLGA. So far, all of the >20 biodegradable polymer-based, long-acting injectable formulations approved by the FDA are based on PLGA due to its long history of safety.[43–45] Drug-loaded PLGA particles are typically produced by the emulsion-based solvent extraction/evaporation method.[43–45] For this production process, effects of processing parameters and formulation compositions on the properties of the products have been extensively investigated in the past three decades. However, due to the complexity of the process and large number of parameters involved, exact relationships between composition/process parameters and product properties remain un-established, and mechanistic understandings are still lacking.[43–45]

Fig. 5 is used to illustrate the complexity of this emulsion-based production process for drug-loaded PLGA particles.[45] Fig. 5 describes the parameters that are known to affect product properties. The composition includes a drug, PLGA polymer(s), and solvent(s). Hydrophobic drugs are mainly considered in this example. Hydrophilic drugs (*e.g.*, peptides and proteins) could be dissolved in water first to form a water/oil/water (W/O/W) emulsion. As shown in Fig. 5, numerous factors contribute to the formation of polymer particles. Inadequate control of the microparticle precursor solution(s) or suspension(s), process parameters, and storage conditions may result in significant variability in the properties of the final formulation.[46,47] For example, the concentration of poly(vinyl alcohol) (PVA), commonly used as a surfactant in the aqueous continuous phase, has a significant effect on the product properties.[48,49] A higher PVA concentration reduces the interfacial tension between organic and aqueous phases yielding smaller particles, but it also leads to faster removal of the solvent to the aqueous phase, producing larger particles. PVA can also account for deformation of microscopic particles.[50] The extraction phase temperature during processing can cause plasticization and annealing of the solid matrix.[51,52] The influences of many factors are self-evident. What is not known, however, is how they exactly impact the properties of the final product, and it is not yet well understood which parameters are more important than others.

Many efforts have been made to improve the controllability and scalability of the emulsion-based solvent extraction/evaporation process for producing drug-loaded polymer particles. For example, Liu *et al.* utilized glass beads in the mechanical stirring process to produce emulsion.[53] At the scale of 60 mg polymer per batch, it was found that the addition of glass beads yielded more homogenous dispersion, and in turn smaller and

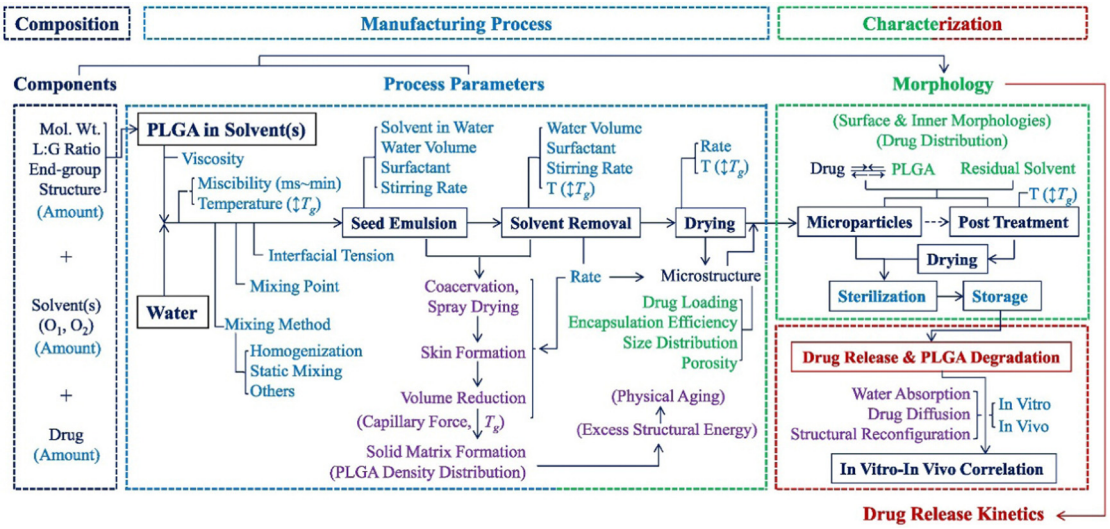

Fig. 5 A flow chart of manufacturing PLGA microparticles by emulsion methods and the parameters affecting the properties of the formulation. Each color represents specific parameters or processes: Dark blue for components, dark blue in a box for main processes, blue for process parameters, purple for physicochemical processes, green for microparticle properties for characterization, and red for drug release characterization. The figure is adopted from ref. 45 with permission.

more monodisperse polymer particles.[53] In another example, Sharifia *et al.* employed in-line homogenization to make the emulsion solvent extraction/evaporation process a semi-continuous one, at the scale of 1–4 g polymer per experiment (Fig. 6).[54]

"Flash technology" is an emerging class of nano-manufacturing methods for polymer microscopic particles, as well as other types of particles. Flash technology involves rapid mixing in confined impingement jets mixers (CIJM) or multiple inlet vortex mixers (MIVM), to facilitate formulation of nano-complexes or nanoprecipitates in a high-throughput and well-controlled manner.[55] CIJM was first developed by Prud'homme and co-workers in 2003.[56] For two-inlet CIJM, two pathways lead to a small chamber where opposing streams containing solvent and non-solvent impinge to create turbulence (Fig. 7a).[57] To maintain continuous flow, syringe pumps drive the streams from syringes into the mixing chamber. A major limitation of CIJM is that the CIJM geometry limits the ratio of solvent to non-solvent due to the requirement for equal momentum of the opposing streams in mixing.[58] To overcome this limitation of CIJM, MIVM was designed to allow unequal solvent-to-nonsolvent ratio mixing in a scalable manner. The concept of the MIVM is that momentum from each stream contributes independently to drive micromixing in the chamber.[58,59] MIVM used in flash technology usually consists of components manufactured using stainless steel and assembled with syringe adapters. MIVM are designed to be

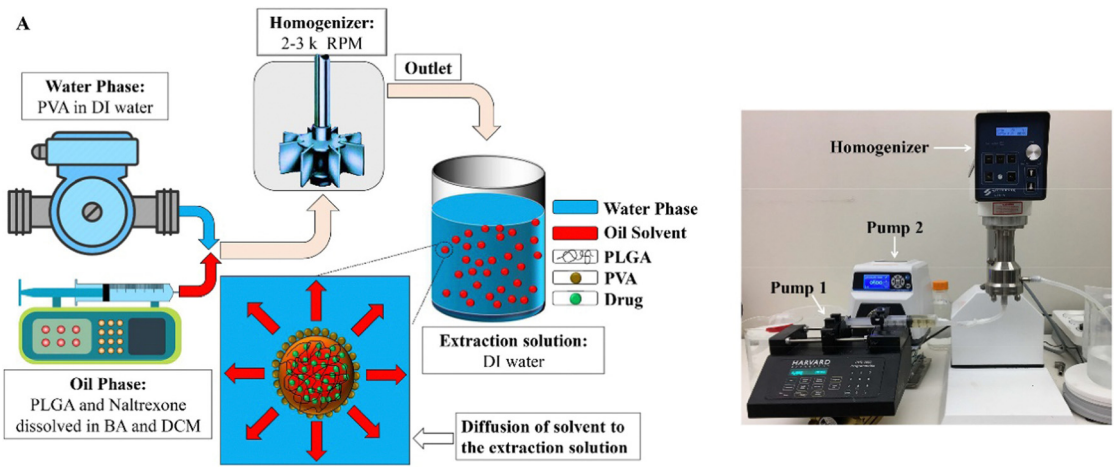

Fig. 6 Utilizing in-line homogenization in the emulsion solvent extraction/evaporation process for producing drug-loaded PLGA particles. (a) Schematic of naltrexone-loaded PLGA generation using an in-line emulsification-extraction process. (b) Experimental set-up used to generate particles by pumping both oil- and aqueous-phases into the homogenizer and transferring the emulsion to the extraction solution. The figure is adopted from ref. 54 with permission.

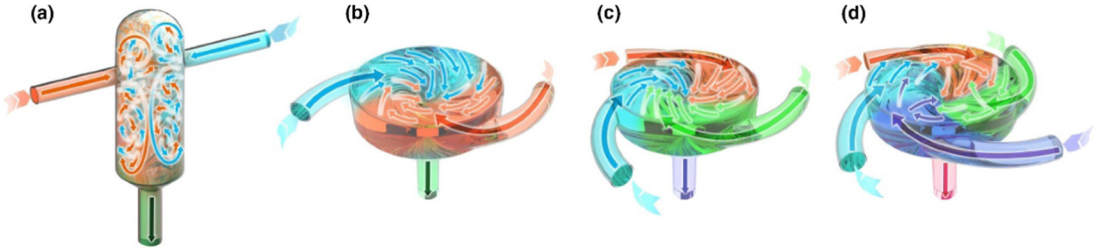

Fig. 7 Geometries of mixers used in flash nanoformulation processes. (a) CIJM, (b) two-inlet MIVM, (c) three-inlet MIVM, and (d) four-inlet MIVM. The figure is adopted from ref. 57 with permission.

easily disassembled and cleaned. 3D printing can be used to fabricate MIVMs.[60] The MIVM design allows the combination of immiscible solutions, providing an additional level of flexibility for nano-manufacturing. The geometries of CIJM and MIVM used in nano-manufacturing are illustrated in Fig. 7.[57] Computational fluid dynamics (CFD) and molecular dynamics (MD) have been used to investigate mixing and reactions in CIJM and MIVM.[61–64] Marchisio and co-workers used CFD modeling to predict mixing in CIJM and MIVM.[65,66] Their work yielded predictions well-correlated with experimental data, and a reliable model for design and scale-up of CIJM and MIVM. Flash technology has seen increasing applications in the past decade for delivery of drugs, proteins, and nucleic acids.[67–75]

Flash technology has been increasingly employed to perform nanoprecipitation, that is, flash nanoprecipitation (FNP). FNP uses rapid micro-mixing to establish homogeneous super-saturation conditions for controlled block copolymer self-assembly and precipitation of hydrophobic solutes.[76] There are several key timescales involved in FNP: mixing time (t_{mix}), nanoformation time (t_{flash}), copolymer aggregation time (t_{agg}), and active organic nucleation and growth time (t_{ng}).[77–79] Controlling t_{mix} is crucial. To obtain homogeneous mixing, the generation of super-saturation by turbulent micro-mixing must be faster than the diffusion-limited aggregation that controls self-assembly. In other words, t_{mix} should be less than the copolymer aggregation time t_{agg} for homogeneous mixing.[77–79] When t_{agg} is close to the nucleation and growth time t_{ng}, the block copolymer interacts with the active particle to alter nucleation and growth and causes colloidal stabilization.[77–79] It has been found that Reynolds number (Re) plays a key role in mixing efficiency, and that Re $>$ 1600 allows sufficient mixing for sub-millisecond FNP reactions.[77–79]

Block copolymer selection is important in formulating stable nanoparticles using FNP. The hydrophobic and hydrophilic regions of block copolymers are balanced so that hydrophobic groups are located mainly in the nanoparticle core. High drug loading is an advantage of FNP self-assembly *versus* slower mixing methods. Fast mixing (high Re) within a chamber provides an ideal niche for supersaturation-induced precipitation of drugs from organic solvent into anti-solvent within milliseconds. This process favors nucleation over particle growth, resulting in smaller and more homogenous nanoformulations. Particle growth is stopped by steric effects caused by the bulky polymeric stabilizer. In contrast, bulk mixing reduces cargo loading efficiency due to unstable drug encapsulation and insufficient stabilizer coverage.

A comparison on product quality and the reproducibility, cost, and scalability of various production processes for organic microscopic particles is shown in Table 1.[22–25,33–38,42,55–59]

Using natural polymers (*e.g.*, albumin) instead of synthetic polymers (*e.g.*, PLGA) to produce particle-based drug delivery systems can take advantage of the inherent biological properties of the natural polymers. For example, for cancer therapeutics, albumin nanoparticles can potentially offer several biological properties inherent to albumin: (1) it is a natural carrier for a number of native molecules and hydrophobic drugs, (2) it is rescued from systematic clearance and degradation by natural mechanisms, (3) it accumulates at sites with vascular leakiness, and (4) it is more greatly taken up and metabolized by cancer cells which are rapidly growing and nutrient-starved.[80] Drug-loaded albumin nanoparticles can be prepared by desolvation with ethanol, sometimes followed by a stabilization step using crosslinking.[81] This method has been established as a standard lab-scale preparation method for albumin nanoparticles. In an effort to extend it to industrial production method, Wacker *et al.* utilized a paddle stirring system to replace the magnetic stirring used in lab-scale preparation.[82] A production scale of 2 gram protein was achieved, with the nanoparticle size ranging between 251.2 $\pm$ 27.0 and 234.1 $\pm$ 1.5 nm and with the polydispersity index

Table 1 A comparison of different production methods of organic microscopic particles for drug delivery

	Particle size	Particle size distribution	Reproducibility	Cost	Scalability
Hand mixing	High	High	Low	Low	Low
Ethanol injection	Medium	Medium	Medium	Low	Low
Membrane-based process	Low	Low	High	Medium	High
Nanoprecipitation	Medium	Medium	Medium	Low	Low
FNP	Low	Low	High	Low	High
3D junction mixer	Medium	Low	High	Low	High
Microfluidics	Low	Low	High	High	Medium

(PDI) below 0.2. In another effort of scalable production, Gopakumar *et al.* employed high-pressure homogenization, yielding gram-scale of albumin nanoparticles encapsulating sorafenib (a small-molecule multi-kinase inhibitor).[83] Further homogenization treatment was conducted to coat a mucoadhesive layer of sodium alginate for enhanced oral delivery of sorafenib.[83] Clinically, the most notable albumin nanoparticle is the so-called nab-paclitaxel (trade name Abraxane®), which is based on high-pressure homogenization of the anticancer drug paclitaxel with albumin, forming nanoparticles with a diameter of roughly 130 nm.[84–86]

Hybrid microscopic particles containing both polymers and lipids have also been explored for biological delivery. In one study, flash technology was used to produce lipid-coated polymer nanoparticles loaded with the anticancer drug doxorubicin.[87] The nanoparticles were made of PLGA and lecithin/1,2-distear oyl-*sn*-glycero-3-phosphoethanolamine (DSPE)-PEG. The mixer was herringbone-patterned, fabricated by 3D printing.[87] In another study using flash technology, MIVM was employed to produce lipid-polymer hybrid nanoparticles, readily achieving production rates of greater than 10 g h^{-1}.[88]

3. Inorganic particle-based delivery systems

3.1 Silica nanoparticles

Silica (SiO_2) nanoparticles have been widely applied as drug delivery systems due to their good biocompatibility, stability, ease of surface functionalization, and possibility to use internal pores to load drug molecules and imaging agents.[89–91] Silica nanoparticles are predominantly prepared by the Stöber method, which was reported by Werner Stöber and co-workers in 1968.[92] The Stöber method is a sol–gel process in which a molecular precursor (typically tetraethylorthosilicate, or TEOS) is first reacted with water in an alcoholic solution, with the resulting molecules subsequently joining together to form larger structures. The above original Stöber process can be modified to prepare porous silica nanoparticles by adding a surfactant template to the reaction mixture and calcining the resulting particles.[89,90] The surfactant forms micelles, around which the silica network grows, forming particles with surfactant- and solvent-filled channels. Calcining the solid leads to removal of the surfactant and solvent molecules by combustion and/or evaporation, leaving porous voids throughout the structure.

A number of efforts have been made to make the Stöber process more scalable. Kim *et al.* modified the Stöber process by using a continuous silica source injection system in a monophasic environment without heating. By doing so the authors synthesized mesoporous silica nanoparticles (MSNs) up to gram-scale with controllable size and narrow size distribution.[93] Flash technology has been adapted to perform the Stöber process. Fu *et al.* utilized a sequential flash technology process to produce abamectin-loaded MSNs (Fig. 8a).[94] Two MIVMs in series were used for forming the micelle template (based on cetyltrimethylammonium bromide, or CTAB) and then MSNs. The silica shell thickness and cavity size were tunable by controlling the composition of reactant streams. Flash technology has also been used for rapid production of ammonium perchlorate (AP) particles. An integrated CIJM system linked to a temperature bath with a peristaltic pump was employed to produce <20 μm AP particles with minimum product clogging at the high rate of 3 kg h^{-1} (Fig. 8b).[95]

3.2 Metal nanoparticles

Thanks to their special optical, mechanical, chemical, and catalytic properties, metal nanoparticles have been widely applied in biomedicine.[96,97] Noble metal nanoparticles such as gold (Au) and silver (Ag) nanoparticles are of particular interest due to their excellent biocompatibility and ease of surface functionalization with biomolecules (*e.g.*, therapeutic or targeting molecules). Furthermore, noble metal nanoparticles possess special plasmonic and photothermal properties which give them potential for applications in biosensing, thermotherapy, and theranostics. Many methods have been developed for the formation of metal nanoparticles. A widely used approach is the chemical reduction route in which aqueous metal ionic precursors are reduced by reducing agents (*e.g.*, ascorbic acid, sodium citrate, and sodium borohydride), and stabilized by polymeric capping agents or surfactants to avoid aggregation.

In an effort to develop scalable production methods for silver nanoparticles, Deshpande *et al.* analyzed the kinetics of silver nanoparticle synthesis *via* citrate reduction in several different reactor configurations, including helical coils, continuous stirred-

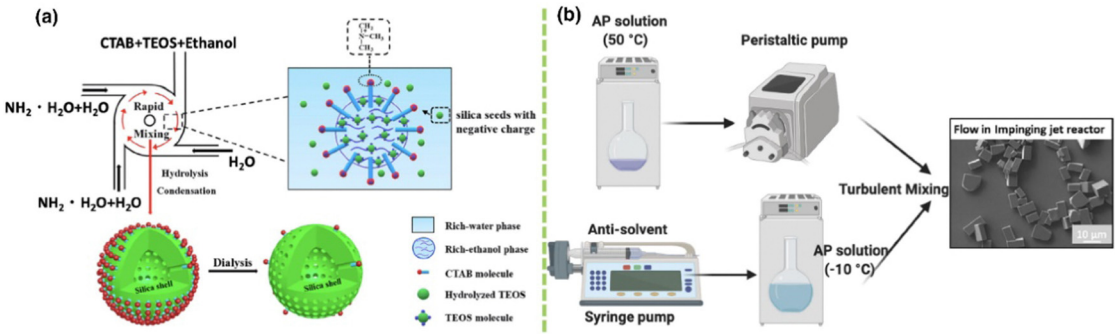

Fig. 8 (a) Production of MSNs by flash technology (adopted from ref. 94 with permission). (b) Flash technology system for the fabrication of ammonium perchlorate particles (adopted from ref. 86 with permission).

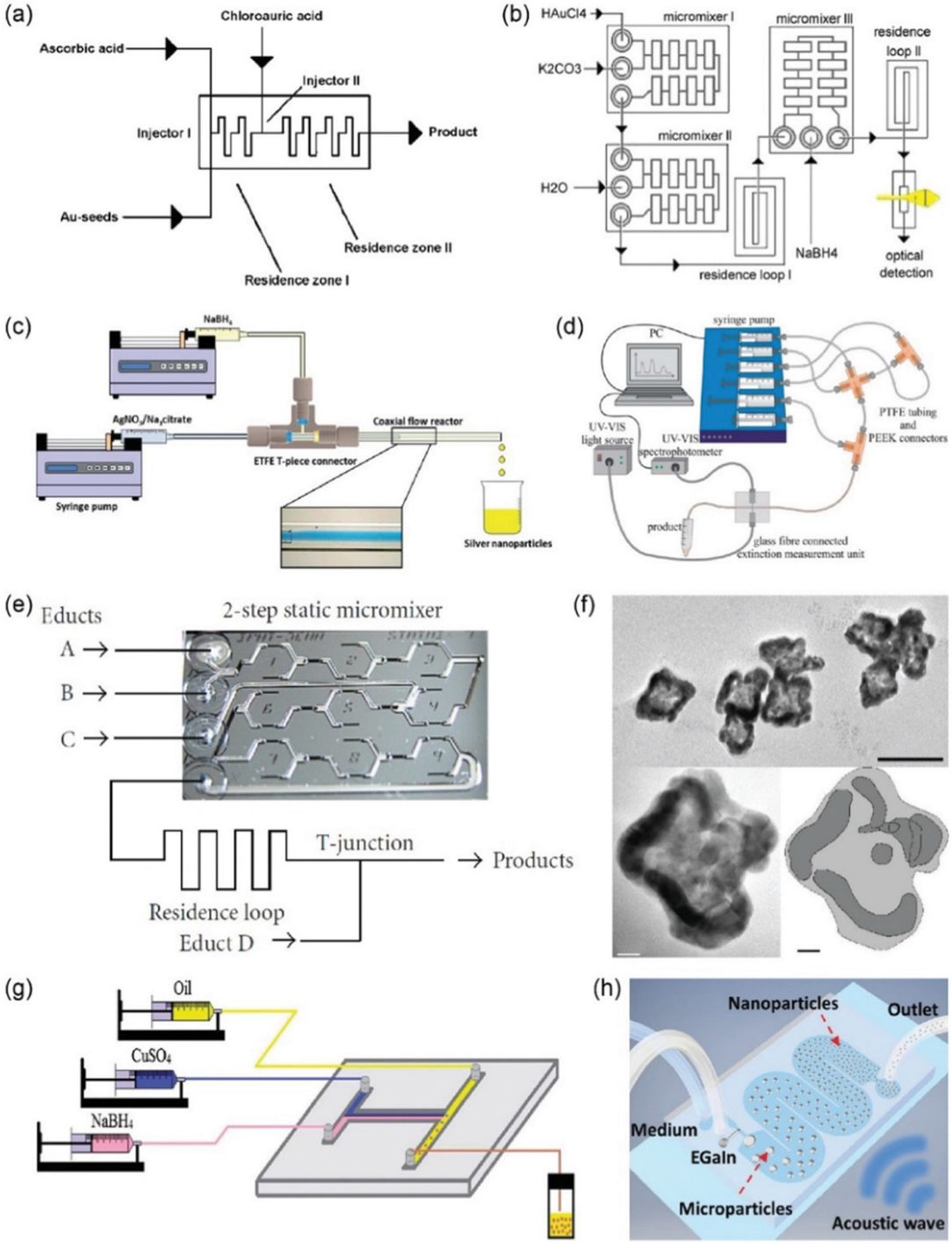

Fig. 9 Microfluidic-based synthesis of metal nanomaterials. (a) Schematic illustration of the experimental set-up and the connectivity of a microfluidic reactor for Au nanoparticle synthesis. Adopted with permission from ref. 99. (b) Schematic diagram of a modular microreactor arrangement for the flow-based synthesis of Au NPs. Adopted with permission from ref. 100. (c) Schematic diagram of the coaxial flow reactor setup. Inset displays flow visualization of laminar flow inside the coaxial flow reactor. Adopted with permission from ref. 101. (d) Schematic diagram of the experimental arrangement for the combinatorial synthesis screening for Ag–shell Au–core NPs. Adopted with permission from ref. 102. (e) Schematic illustration of the experimental arrangement for the microflow-based synthesis of core–shell nanoparticles (A, B, C, D, . . . inlet ports for educt solutions). Adopted with permission from ref. 103. (f) Transmission electron microscopy images and an interpretation scheme (bottom right) of star-like Au/Ag nanoparticles. Adopted with permission from ref. 103. (g) Schematic of the synthetic processes of Cu nanoparticles by a T-shaped microflow chip at room temperature. Adopted with permission from ref. 104. (h) Schematic representation illustrating the working mechanism of liquid metal NP formation, where liquid metal microdroplets formed at the T-junction are later gradually broken into NPs in the presence of acoustic waves. Adopted with permission from ref. 107.

tank reactor (CSTR), CSTRs in series, segmented-flow reactor, and 3D flow reactor.[98] It was found that having a larger CSTR at the beginning of the series of CSTRs was not suitable, because nucleation is a fast reaction and at least one small CSTR should be used exclusively for the nucleation phase to avoid a significant overlap of nucleation and growth. It was also found that a higher number of tanks enhanced the reaction rate, conversion, and hence, the particle sizes. The effects of backmixing, initial reaction concentration, pH, and temperature on the reaction conversion, particle size, and poly-dispersity were quantified and used for the identification of a suitable reactor configuration. Mixing, *i.e.*, extent of dispersion, was found to have a strong impact on the overall conversion rates as well as the particle size distribution.

Microfluidics-based production methods have been developed for the synthesis of metal nanoparticles. By using 12 nm sized, citrate-stabilized Au NPs as seeds, Wagner *et al.* synthesized larger Au NPs with diameters from 15 to 24 nm using a continuous flow microfluidic reactor (Fig. 9a).[99] In the reactor, $HAuCl_4$ was reduced by ascorbic acid, leading to the growth of Au NPs, which was further stabilized using polyvinyl pyrrolidone (PVP).[99] These authors also reported synthesis of ultrasmall Au nanoparticles (4 to 7 nm) directly from precursor solutions under continuous flow conditions (with the highest flow rate tested being 4 mL min^{-1}).[100] Rather than using smaller Au NPs seeds, an Au salt ($HAuCl_4$) solution, a reducing agent ($NaBH_4$), and a ligand were pumped separately from different inlets into a glass-silicon microreactor system consisting of three static chip micromixers, which led to the formation and direct surface modification with thiol ligands of Au NPs (Fig. 9b).[100] Two approaches, namely (1) hydrophobic treatment of the reactor and (2) the elevation of pH, were utilized to suppress Au nucleation at the inner channel surface, which could potentially cause channel clogging.[100] The channel blockage issue can also be eliminated by using microfluidic coaxial flow reactors, in which nucleation and growth of nanoparticles are confined at the interface of the inner and outer flows away from the channel walls. For example, by using an ETFE T-piece connector, Baber *et al.* synthesized Ag nanoparticles with $AgNO_3$ and $NaBH_4$ being the inner and outer streams, respectively, in the presence of trisodium citrate as the surfactant (with the highest flow rate tested being 14 mL min^{-1}) (Fig. 9c).[101]

In addition to single-phase nanoparticles, binary composed noble metal nanoparticles can also be fabricated using microfluidics. Knauer *et al.* synthesized Ag–shell Au–core nanoparticles using a segment flow microreactor system, in which Ag was reduced from its precursor salt solution and uniformly grew on Au nanoparticle seeds to form a homogeneous 1.1–6.1 nm layer (with the highest flow rate tested being $\sim$100 μL min^{-1}) (Fig. 9d).[102] Using a continuous flow microreactor with multiple inlets at different locations (Fig. 9e), Au/Ag nanoparticles with star-like and core–shell structures were prepared by directly reducing Au and Ag salts with ascorbic acid (with the flow rate used for $HAuCl_4$ being 0.5 mmol L^{-1}) (Fig. 9f).[103] By controlling the concentration of the reducing agent, the relative nucleation rate of Au and Ag can be adjusted, leading to the different spatial distribution of elements inside the nanoparticles.

In addition to noble metals, efforts have also been made to utilize microfluidics to prepare other metal nanoparticles including Cu, Pd, and Gd, *etc.*[104–106] For example, Cu NPs were prepared by reducing $CuSO_4$ with $NaBH_4$ under a segmented flow condition using a T-shaped microfluidic chip (with the flow rate used for $CuSO_4$ being 0.2 mol L^{-1}) (Fig. 9g).[104] By using PVP as the dispersant and antioxidant, Cu nanoparticles were prepared with their size, morphology, and size distribution and elemental compositions regulated by the flow rates. The synthesis of liquid metal nanoparticles using microfluidics was also reported recently. Due to the large surface tension of liquid metals relative to water, it is challenging to create fine liquid metal nanoparticles solely by the shear force provided by a T-junction. In this regard, Tang *et al.* embedded the T-shaped microfluidic channel into a sonication bath to break the eutectic gallium indium (EGaIn) liquid metal microparticles into NPs using an acoustic wave (with the reported yield reaching 50 mg mL^{-1}) (Fig. 9h).[107]

3.3 Metal oxide nanoparticles

Metal oxide (*e.g.*, titanium oxide and iron oxide) nanoparticles have found many biomedical applications such as tissue engineering, bio-imaging, immunotherapy, and drug delivery. For example, TiO_2 nanoparticles have been utilized for tissue engineering due to their excellent biocompatibility and cell adhesion ability. Iron oxide nanoparticles have been applied for magnetic resonance imaging (MRI), magnetically-guided drug delivery, and hyperthermia.[108–110] High quality iron oxide nanoparticles are most commonly synthesized by the thermal decomposition method.[111] In this method, organometallic precursors are used to produce monodispersed nanoparticles under high temperature. The process of decomposition of organometallic precursors is carried out under the presence of organic stabilizing agents to produce iron oxide nanoparticles of the desired size and shape. The stabilizing agents used include fatty acids, hexadecylamine, and oleic acid. The stabilizers can slow down the nucleation of nanoparticles and help in producing a spherical shape and desirable size of less than 30 nm (often $<$10 nm).

Microfluidics has been adapted to synthesize iron oxide nanoparticles, using both tubular and chip-based micro-reactors *via* the coprecipitation mechanism, which relies on the pH-dependent solubility of iron oxides. At a pH above 10, iron salt solutions become supersaturated, triggering the nucleation and growth of the iron oxide nanoparticles in the solution.[112] Using a continuous flow micro-reactor, iron oxide nanoparticles with sizes between 26.5 and 34 nm were synthesized through the oxidative hydrolysis of Fe^{2+} salts (with the flow rate used for iron precursor being 3.25–9.75 mol min^{-1}).[113] The two modular unit designs allowed control of the type of gas dissolved in the solution (Fig. 10a). In another effort, iron oxide nanocrystals with diameter ranging from 23 to 70 nm were prepared *via* segmented flow using a gas slug microfluidic reactor, in which mixing and reaction stages were segregated for fast mixing of precursor solutions as well as precise control over the reaction temperature and atmosphere (with the flow rate used for the iron precursor being 0.22 mol min^{-1}) (Fig. 10b).[114] The type of gas slug was found to play an important role in regulating the morphology of iron oxide

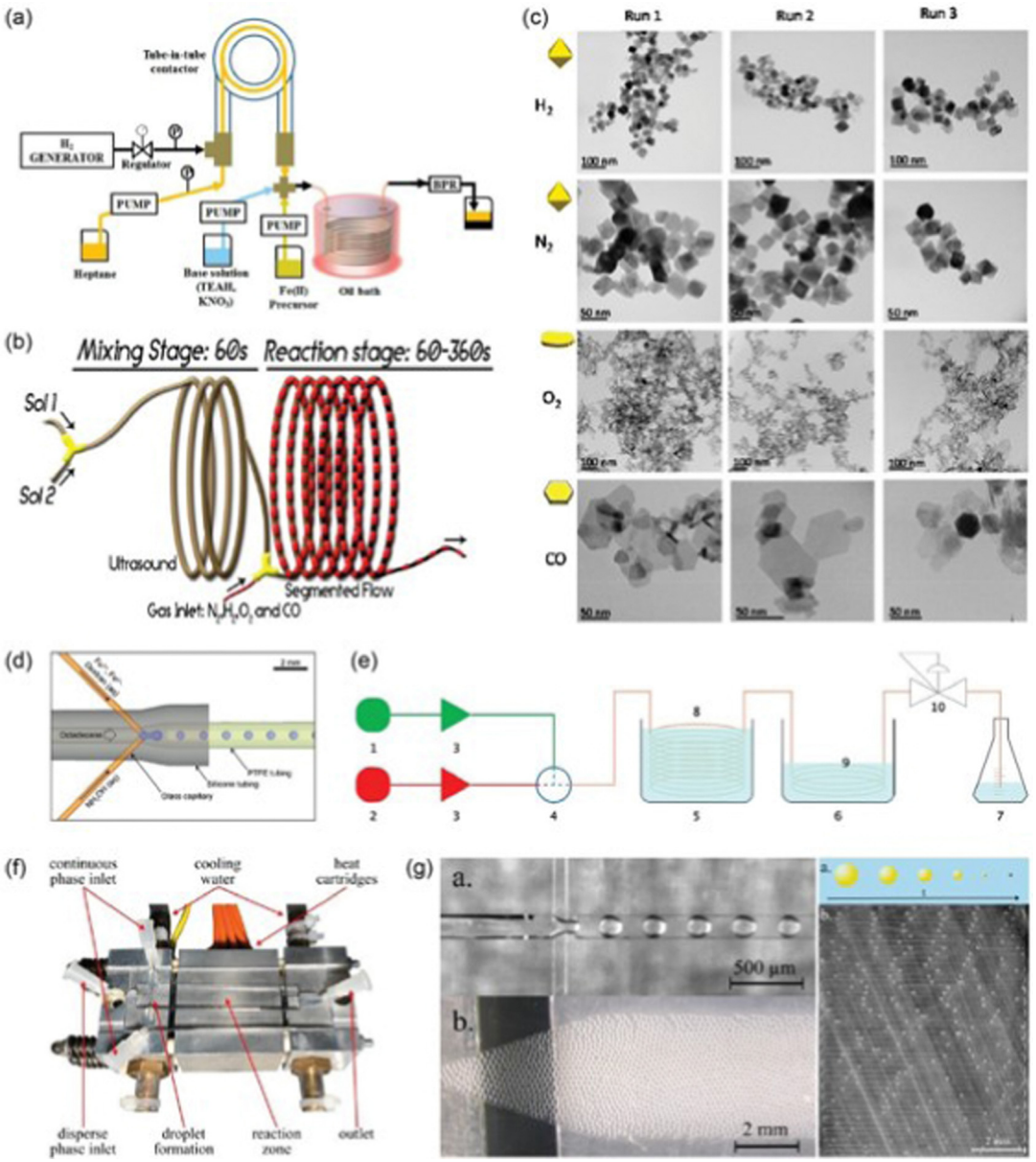

Fig. 10 Microfluidic-based synthesis of metal oxide nanomaterials. (a) Schematic of the experimental setup with H_2-saturated heptane for flow synthesis of iron oxide nanoparticles. Adopted with permission from ref. 113. (b) Schematic diagram of the microfluidic setup designed to produce magnetic nanoparticles in gas–liquid segmented flow. Adopted with permission from ref. 114. (c) Transmission electron microscopy images of magnetic nanoparticles obtained using the microfluidic setup in (b) at different runs and under different gas environments (H_2, N_2, O_2, and CO). Adopted with permission from ref. 114. (d) Schematic of the capillary-based segmented flow reactor showing the injection of precursor solutions of Fe^{2+}/Fe^{3+}/dextran and NH_4OH into a continuous octadecene stream for the synthesis of iron oxide NPs. Adopted with permission from ref. 115. (e) Schematic diagram of the experimental setup for the preparation of TiO_2 nanoparticles (1—$CO(NH)_2$ solution, 2—$TiOSO_4$ solution, 3—advection pumps, 4—micromixer, 5—oil bath, 6—water bath, 7—triangle beaker, 8—steel tube for heating, 9—steel tube for cooling, 10—back-pressure regulator). Adopted with permission from ref. 116. (f) Photograph of the temperature controlling module mounting with a microfluidic chip. Adopted with permission from ref. 117. (g) Droplet formation of precursor and benzyl alcohol in Fluoronox inside the microfluidic device (left) and the dissolution of benzyl alcohol in the continuous phase causing droplet shrinkage over time (right). Adopted with permission from ref. 117.

nanoparticles, with H_2 and N_2 slugs leading to cubic nanoparticles, and O_2 and CO slugs resulting in spherical/rod and hexagonal nanoparticles, respectively (Fig. 10c). Iron oxide nanoparticles coated with a polymer layer were also prepared using microfluidic devices. By using aqueous solutions of Fe^{2+}/Fe^{3+}/dextran and NH_4OH as the two precursor solutions to induce the co-precipitation of iron oxide in a capillary-based droplet reactor, Kumar *et al.* obtained dextran-coated superparamagnetic iron oxide nanoparticles with a mean diameter of 3.6 nm and narrow size distribution (with the carrier flow rate used being 600 μL min^{-1}) (Fig. 10d).[115] TiO_2 nanoparticles have been extensively fabricated through a hydrothermal process, in which the TiO_2 precursors crystalize at high pressure and relatively low temperature, thus leading to low agglomeration, finer particle

sizes, and narrower size distribution compared to other conventional procedures that require calcination.[116] However, a long reaction time is normally required for the preparation of TiO_2 nanoparticles due to the low thermal transmission rate and slow hydrolysis of organic titanium reagents. This problem can be addressed by preparing TiO_2 nanoparticles using a microfluidic reactor. For example, Deng *et al.* synthesized superfine TiO_2 nanoparticles using a microcurved-tube system (with the flow rate used for the Ti precursor being 0.3 g min^{-1}) (Fig. 10e).[116] By utilizing a droplet-based segment flow microfluidic reactor integrated with a computer-controlled heating and cooling system, Stolzenburg *et al.* reported the synthesis of multiple types of metal oxide nanoparticles (with the flow rate used for the metal precursor being 180 mmol L^{-1}) (Fig. 10f and g).[117]

3.4 Quantum dots

Semiconductor nanocrystals, also known as quantum dots (QDs), exhibit unique fluorescent properties, such as high fluorescence intensity, photo-stability, narrow fluorescence peak width, size-dependent fluorescence peak wavelength, and long fluorescence lifetime. QDs have found numerous biomedical applications such as bio-imaging, diagnostics, and drug delivery.[118] The most successful and widely adopted QD syntheses involve rapid nucleation by injection of a precursor into a hot bulk liquid, followed by growth at a lower temperature in the presence of stabilizing surfactants.[119] This process is usually performed in a batch reactor. There have been efforts to scale up the batch reaction.[120,121] In one example, the Peng team introduced the SILAR (successive ion layer adsorption and reaction) process, which was originally developed for deposition of thin films on solid substrates from solution baths, to grow high quality QDs at large scale (2.5 gram per batch).[120] In another example, the Zhong team reported a non-injection method to synthesize QDs at gram-scale (>3 g per batch).[121]

Meanwhile, there have been an increasing number of reports on adopting microfluidics to produce QDs. The earliest works on microfluidics synthesis of QDs were conducted by the deMello team[122] and the Alivisatos team.[123] Soon afterwards, the Mathies and Alivisatos team developed a droplet-based microfluidics platform for synthesis of QDs.[124] In the microfluidics design, the authors used a stepped microstructure to reproducibly generate controlled streams of octadecene droplets (Fig. 11). CdSe nanocrystals were synthesized at high temperature in this droplet-based micro-reactor. Many efforts have been made since these early reports.[125]

Electrospray-based methods have been employed for semi-continuous production of hybrid nanoparticles containing polymers, QDs, and sometimes also iron oxide nanoparticles.[126–130] In these reports, a top-down process, namely co-axial electrospray, and a bottom-up process, namely interfacial instability-induced self-assembly, were combined to form inorganic–organic hybrid nanoparticles with sub-100 nm sizes (Fig. 12).

3.5 Microorganisms-based production

Although chemical methods are more established, microorganisms-based methods have the potential to offer cheap, scalable and highly tunable green synthetic routes for the production of nanomaterials.[131] In an example of biosynthesis of silver nanoparticles as antimicrobials, Fayaz *et al.* utilized *Trichoderma viride* to synthesize silver nanoparticles from silver nitrate solution.[132] The nanoparticles were formed *via* naturally occurring reductants in culture filtrates. Bacterial systems have also been studied for biosynthesis of silver nanoparticles. The subsurface iron-reducing bacterium *Geobacter sulfurreducens* has been shown to reductively precipitate extracellular silver nanoparticles.[133] In an example of biosynthesis of iron oxide nanoparticles, Moon *et al.* employed *Thermoanaerobacter* sp. TOR-39 to produce biogenic zinc-doped magnetite (Fe_3O_4) nanoparticles with large quantity (1 kg wet weight).[134] In an example of biosynthesis of gold nanoparticles, Hassanisaadi *et al.* evaluated the extracts of 109 different plant species as possible sources of gold nanoparticles. 37 of them were found to result in biosynthesized gold nanoparticles, with sizes ranging from 27 to 107 nm.[135] In an example of biosynthesis of QDs, Bao *et al.* used *E. coli* to synthesize cadmium telluride (CdTe) QDs with tunable fluorescence emission.[136] The QD precursors (cadmium chloride, trisodium citrate, Na_2TeO_3, mercaptosuccinic acid, and sodium boronhydride) were mixed with *E. coli* cells. As the CdTe crystals formed from chemical reduction of the tellurite by the boronhydride, extracellular proteins from the microbial cultures were thought to play a critical role in QD crystal growth, ultimately forming a biocompatible capping layer around the nanoparticles. The large gene pool of microorganisms has the potential to encode enzymatic systems that can yield synthesis of many different nanomaterials. As understanding of the underlying biochemistry and genetics of these microorganism systems is increasingly developed, these biosynthesis-based production methods are expected to become an important component of our synthetic biology toolbox.

4. A comparison of the production of organic and inorganic microscopic particles

The formation of organic microscopic particles often involves inter-molecular forces such as van der Waals forces, electrostatic forces, steric and depletion forces, hydrogen bonds, and hydrophobic interactions.[137] Bottom-up formation (self-assembly) of these particles is predominantly driven by inter-molecular forces. Top-down fabrication processes of these particles often involve some degree of inter-molecular forces, coupled with other forces (*e.g.*, high shear stress-induced droplet breaking). Self-assembly is driven by the lowest energy principle. Individual components are driven by various intermolecular forces in the direction of minimum energy, and the components are assembled into an orderly, stable structure. In principle, self-assembly processes should be highly reproducible and easy-to-control, since the state of the product is supposedly determined by the minimum energy.[138] However, in practice, the mechanism of self-assembly is not well understood at present, and this is an important reason why the critical process parameters (CPPs) in self-assembly processes are difficult to identify. It has been

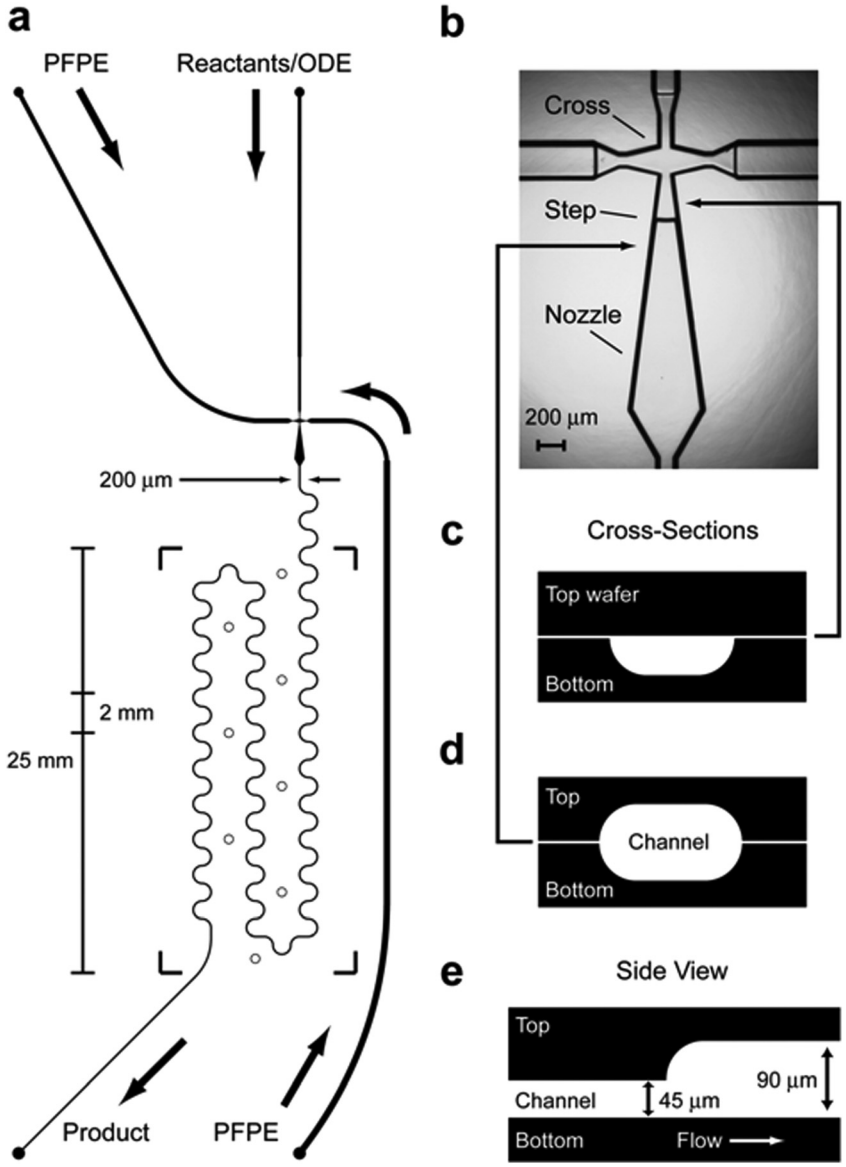

Fig. 11 Micro-reactor channel design with droplet jet injector. (a) Channel schematic showing dimensions, inlets (·), thermocouple wells (○), and boundaries of Kapton heater (square brackets). (b) Optical micrograph of droplet injection cross. Octadecene is injected in the top channel, while the PFPE is injected in the side channels. The narrowest point is 160 μm wide. (c) Lateral "D"-shaped cross-section of channel etched on the bottom wafer only. (d) Cross-section of ellipsoidal channel etched on both top and bottom wafers. (e) Axial cross-section showing the 45 μm step up in channel height. This figure was adopted from ref. 124 with permission.

found that structures that are metastable can be stabilized during dynamic self-assembly.[139] When it comes to scalable production, when the mass transfer efficiency is low, several metastable structures may co-exist in the system. Moreover, some self-assembly processes are very fast, which places high demand on mass transfer of the mixing process.[140]

In laboratory scale production, due to the small volume of the reactor, heat and mass transfer is often not problematic. However, in the pilot scale, the heat and mass transfer problem becomes significant. Two different approaches have been used to solve this problem. One approach is to stick to the amplified reactor, and try to choose the appropriate stirrer (*e.g.*, propeller, turbine, paddle, anchor, frame, and screw) with the appropriate stirring speed. During the scale-up process, the pilot scale production needs to reproduce the reaction rate, yield, and product quality from the laboratory scale production. The main influencing factors often include temperature, concentration, mass transfer, and shear rate. It is often not possible for all four to be identical for reactions of different sizes. The scale-up process can sometimes be simplified by making some choices from these influencing factors. For example, self-assembly is usually performed at room temperature, thus temperature can be removed from the list of the main influencing factors. Another approach is to use continuous production in relatively small reactors. The small reactor size allows mass and heat transfer to be similar to that of laboratory scale production,

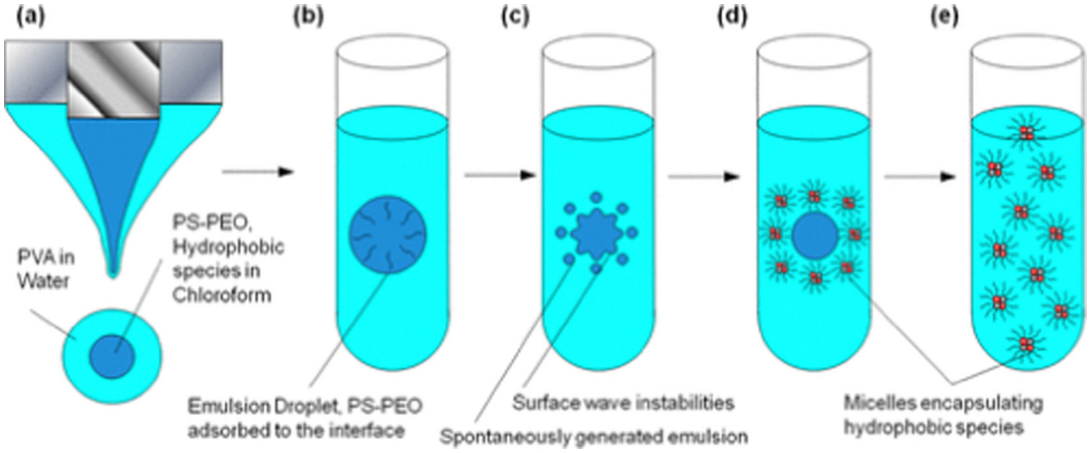

Fig. 12 Schematic diagram of the key steps in the micellar electrospray synthesis process. (a) The coaxial electrospray generates a compound aerosol droplet containing PS–PEO and hydrophobic species dissolved in chloroform and PVA dissolved in water. The aerosol droplets are collected in a larger water bath to yield (b), the organic emulsion droplets. PS–PEO will adsorb to the emulsion droplet interface resulting in (c), an emulsion droplet with surface wave instabilities that spontaneously eject smaller emulsion droplets. The smaller emulsion droplets undergo further interfacial instabilities until they form (d), micelles encapsulating the hydrophobic species. Complete removal of the organic solvent through instabilities and evaporation results in (e), a suspension of micelles containing hydrophobic species. This figure is adopted from ref. 126 with permission.

thereby better reproducing the product quality, reaction rate, and yield.

On the other hand, formation of inorganic microscopic particles often involves crystallization processes, which include the stages of atom generation, nucleation, and crystal growth.[141] The first step, atom generation, often involves redox reactions. The second step (nucleation) and the third step (growth) tend to overlap. The explosive and continuous nature of nucleation is the main reason why the crystallization processes are difficult to control, and is a major obstacle limiting the mass production. The crystal growth is slowed down and controlled by capping of organic stabilizers.[142] Reducing the degree of overlap between the nucleation and growth steps can improve the homogeneity of the products. In addition, the growth rate of larger particles is slower than that of smaller particles, thus increasing mass and heat transfer in the crystal growth step could improve the product homogeneity.

5. Downstream processing after production

5.1 Purification

In the early stage of product development, purification of microscopic particles is usually performed on a laboratory scale using centrifugation or dialysis, requiring manual processing which is difficult to achieve reproducibility. To date, the first technologies that have been developed for the scalable purification process of microscopic particles include membrane separation (tangential or cross-flow filtration) and continuous flow centrifugation.[143]

Tangential flow filtration (TFF) is a continuous filtration method in which the fluid flows along the membrane surface rather than through the membrane, resulting in less particle accumulation on the membrane surface and more stable filtration rate. TFF also allows the gradual exchange of solvents into isotonic solutions that can be further concentrated for subsequent applications. Liu *et al.* synthesized pDNA/lPEI nanoparticles by flash technology, and performed scalable purification based on TFF to reduce the concentration of free PEI in the nanoparticle formulation (Fig. 13).[144] TFF was found to reduce free PEI by 60% while preserving the size and morphology of the nanoparticles. Furthermore, a comparison with the ultrafiltration method showed significant superiority of TFF in nanoparticle product size, DNA recovery, and free PEI remaining in the product (Fig. 13).[144]

Continuous flow centrifugation is a centrifugation technique suitable for large-scale preparation where the sample liquid is continuously introduced into the centrifuge, the precipitation is kept in the centrifuge bin, and the supernatant is discharged continuously. Many types of continuous centrifuges are available, which are named after their geometric features such as perforated bowl centrifuges, scroll discharge centrifuges, and tubular centrifuges. They have been used in a variety of applications including biomaterials, cells and vaccines.

High-speed centrifugal machines (centrifuges) with a solid elongated bowl (length-to-diameter ratio of L/D = 5–7, Fig. 14) are used in many industrial sectors.[145] In this kind of tubular bowl centrifuge, the feed enters the centrifuge under pressure through a nozzle at the bottom, and is accelerated to rotor speed, then moves up the cylindrical bowl. The solid is removed from the liquid if it moves to the top of the bowl wall at a sufficient speed during the residence time of the liquid in the machine. Solids in tubular centrifuges are accelerated by forces between 13 000 and 16 000 times the force of gravity. Ultracentrifuge, a form of narrow tubular bowl centrifuge, is used to break down emulsions and creates a centrifugal force 105 to 106 times higher than gravity. The RTR-102K-01 and RTR-151K-01 tubular centrifuge models are used for continuous separation of emulsions. Bowl diameters of these industrial

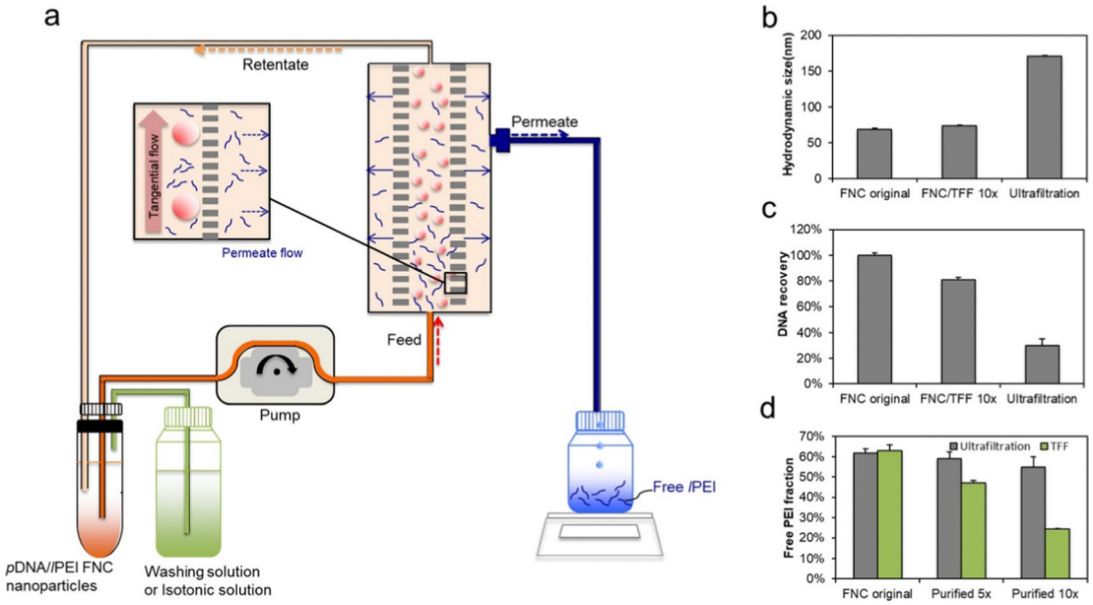

Fig. 13 (a) Schematic diagram of pDNA/lPEI nanoparticle purification by TFF. Comparison of (b) *z*-average hydrodynamic size, (c) DNA recovery, and (d) free lPEI fraction of the nanoparticles before purification (FNC original nanoparticles) *vs.* following purification by TFF and ultrafiltration methods using the 5 volume washing (5×) and 10 volume washing (10×) protocols, respectively (n = 3). The 5× and 10× washing refers to 5 and 10 times of the volume of the solvent used, respectively, in reference to the volume of nanoparticles. This is measured by the volume of the permeate collected during the TFF process. This figure is adopted from ref. 144 with permission.

centrifuges range from 80 to 150 mm and their processing capacities range from 0.2 to 2.0 $m^3\ h^{-1}$.[145]

Another type of tubular centrifuge used in industry is a disc stack bowl centrifuge.[146] Under the influence of centrifugal force, the heavier feed components are thrown outward, while the lighter liquid is moved toward the center of the bowl, flows inward through the upper face of the disc, and is expelled from the top of the bowl (Fig. 15).[146] One drawback of centrifuges that automatically expel solids is that the solids must remain wet enough to flow through the machine. Disk-stacked centrifuges used for biological processing typically produce forces between 5000 and 15 000 times gravity. For reference, the minimum solid–liquid density difference for successful separation in a disk-stacked centrifuge is about 0.01 to 0.03 $kg\ m^{-3}$. In practice, the smallest particle diameter separated is about 0.5 μm at an appropriate flow rate.[147]

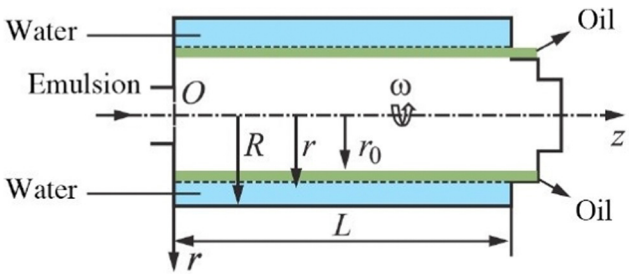

Fig. 14 Schematic for calculating the oil-in-water emulsion separation process in the bowl of a continuous centrifuge. This figure is adopted from ref. 145 with permission.

5.2 Bioconjugation

Conjugation of microscopic particles with biomolecules, such as antibodies or drugs, can potentially offer further targeting or therapeutic abilities. Wicki *et al.* reported their large-scale, GMP-compliant production process of doxorubicin-loaded and anti-EGFR-coated immunoliposomes (anti-EGFR-ILs-dox) used in a first-in-man, dose escalation clinical trial.[148] Ten batches of this nanoparticle were produced in clean room facilities. All batches fulfilled the defined release criteria, indicating a high reproducibility as well as batch-to-batch uniformity of the main physicochemical features of the nanoparticles in the setting of the large-scale GMP process. The monoclonal antibody and PEGlated liposomal doxorubicin (PLD) were modified in a 5-day production process (Fig. 16).[148] The antigen-binding fragment (Fab') of the antibody was covalently conjugated to the maleimide group at the terminus of the PEGylated distearoylphosphatidylethanolamine chain (DSPE-PEG-MAL3400). Through co-incubation of PLD and conjugated Fab' fragment of the anti-EGFR-antibody at the specific phase-transition temperature of PLD (59 °C), conjugated Fab' was integrated into the phospholipid bilayer membrane of PLD *via* its DSPE group. In another example, van der Put *et al.* reported the scale-up feasibility under GMP conditions of a high yielding bioconjugation process for SF2a-TT15, a glycoconjugate vaccine candidate targeting *Shigella flexneri* 2a (SF2a).[149] SF2a-TT15 is made of a synthetic 15 mer oligosaccharide, corresponding to three non-O-acetylated repeats, linked at its reducing end to tetanus toxoid by means of a thiol-maleimide spacer.

Developers of bioconjugation for microscopic particles could learn from a related, and more established field in industry, *i.e.*, antibody-drug conjugates (ADC).[150,151] For example, in the evolution history of the ADC field, linker optimization has

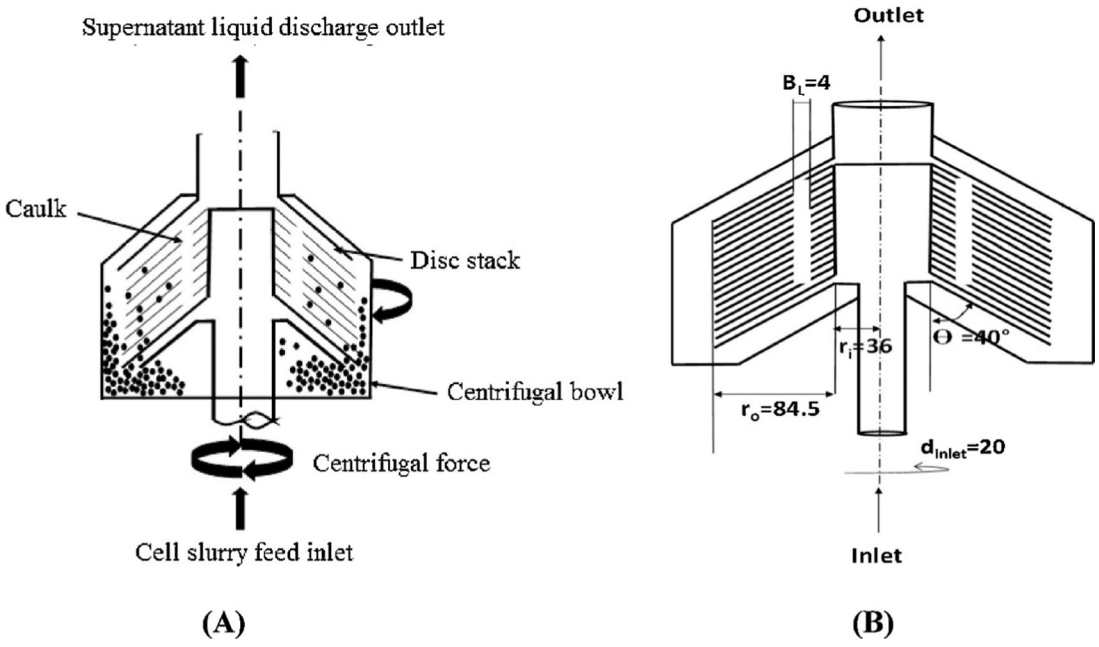

Fig. 15 (a) Schematic of a disc stack centrifuge (DSC) and (b) dimensions (in mm) of the disc stack centrifuge (DSC). This figure is adopted from ref. 146 with permission.

proven to be key. Linkers must be stable while the ADC is circulating in the blood to limit off-target toxicity, but allow for release of the drug once it is inside the target cells. It has been shown that the blood stability of the older generation ADCs is limited.[152] Most second-generation ADCs in clinical development have maleimide-type linkers and undergo a so-called deconjugation phenomenon in the serum, which results in off-target cytotoxicity. Efforts have been made to address it in the newer generation ADCs. In order to form a stable linker, it has been reported that drugs can be conjugated either through intra-strand sulfhydryl linkages, genetically engineered unnatural amino acids, or the epsilon amino groups of lysine.[153] Different linkers can be selected based on the target physiological environment in which the drug needs to perform its bioactivity. If the target environment is acidic (*e.g.*, tumor microenvironment), acid-labile hydrazones can be selected as the linker, while for a

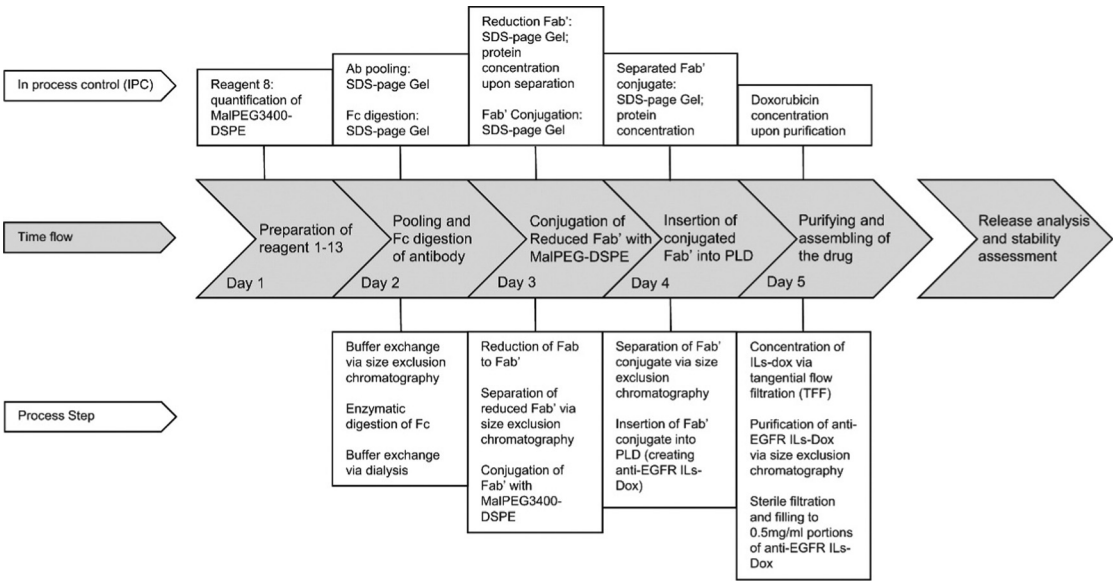

Fig. 16 Production cycle of a GMP batch of anti-EGFR ILs-dox: Anti-EGFR ILs-dox was manufactured in a 5 day production process. The key achievements of each production day are indicated in the gray, arrow-shaped time flow textboxes. Conducted process steps and in process controls (IPC) are linked to the corresponding day in the above IPC line and underneath process step line, respectively. This figure is adopted from ref. 148 with permission.

reductive environment (*e.g.*, cytoplasm), disulfide linkers are preferred.[154] Another major trend in the ADC field is the engineering of IgG molecules to allow for linkage with cytotoxic molecules at defined positions that are suitable for drug conjugation and thus to obtain more homogeneous drug conjugates. The instability of ADCs in the circulation may also be overcome by alternative bioconjugation chemistries in combination with optimal antibody engineering.[155] As a result, more than 40 site-specific drug conjugate technologies, which are often combined with alternative conjugation chemistries, have been developed, and at least 10 ADCs that are based on these technologies have reached clinical development. The main objectives of these technologies are to enhance homogeneity and to reduce the drug deconjugation rate in the circulation to limit off-target toxicity, thereby increasing the delivery of highly cytotoxic drugs to tumors while also improving tolerability. An example of developing a Good Manufacturing Practice (GMP) process for site-specific linkage of ADC can be found in Matsuda *et al.*'s report.[156]

5.3 Sterilization

Finding an appropriate sterilization method is a crucial step for microscopic particles to be used within human bodies. The sterilization method for each nano/miro-formulation needs to be developed and validated on a case-by-case basis, as microscopic particles can be affected differently by the sterilization method depending on the components and preparation method.[157] Sterilization procedures such as gamma irradiation, ultraviolet light, or autoclaving could be detrimental to sensitive active pharmaceutical ingredients (APIs), cause chain alteration of polymers (*e.g.*, PLGA), and affect the overall characteristics of the nanoformulation itself.[158–161] However, there have also been publications reporting that gamma irradiation caused no significant changes to PLGA particle-based drug formulations.[161,162] If gamma irradiation, ultraviolet light, and autoclaving are found to be problematic, an alternative method can be sterile filtration of the final product. Nevertheless, this process only works for nanoformulations with a size distribution smaller than 0.22 μm. Finally, aseptic manufacturing can be implemented. However, aseptic processes can be costly and difficult to perform particularly for multi-step processes.[157,163]

5.4 Storage

Colloidal particles are often stored in liquid form at 2–8 °C. In addition to the degree of purity, the physicochemical integrity of a microscopic particle-based drug formulation needs to be preserved over time throughout its shelf-life. During storage, these microscopic particles can be subjected to aggregation and degradation pathways mediated by light, oxygen, heat and water. Lyophilization (freeze-drying) is a commonly used method to improve long-term storage stability of colloidal particles. Lyophilization can prevent drug leakage, avoid the weakening of drug activity, and minimize the degradation of the carrier material. In the process of lyophilization, lyophilization protective agents can be added. These agents include alcohols (glycerin, mannitol, sorbitol, inositol, xylitol, vitamin D, vitamin E), sugars (glucose, sucrose, trehalose, starch, lactose, maltose), amino acids (glutamic acid, arginine, histidine, serine, alanine, gelatin), and salts (phosphate salt, citric acid, acetic acid salt).[164] Recently, continuous freeze-drying and continuous aseptic spray-drying have been proposed for future continuous manufacturing of nanomedicines.[143,165–167]

Author contributions

H. L., J. L., and P. F. wrote the first draft of the manuscript. Z. X. and G. R. supervised and edited the writing. H. L.: writing – original draft (the 'Organic particle-based delivery systems' section, and part of the 'downstream processes' section). J. L.: writing – original draft (the 'Inorganic particle-based delivery systems' section). P. F.: writing – original draft (part of the 'downstream processes' section). Z. X.: writing – review and editing. G. R.: conceptualization. Supervision. writing – review and editing.

Conflicts of interest

The authors declare no conflict of interests.

Acknowledgements

The authors acknowledge the financial support from Jiangsu Natural Science Foundation (No. BK20171259), Nantong Natural Science Foundation (No. JC2019045, JC2019049), and XJTLU Research Development Funding RDF-21-02-007.

References

1 W. Poon, B. R. Kingston, B. Ouyang, W. Ngo and W. C. W. Chan, A Framework for Designing Delivery Systems, *Nat. Nanotechnol.*, 2020, **15**, 819–829.
2 The Delivery Problem, *Nat. Biotechnol.*, 2006, **24**, 305–306, DOI: **10.1038/nbt0306-305b**.
3 H. Park, A. Otte and K. Park, Evolution of drug delivery systems: From 1950 to 2020 and beyond, *J. Controlled Release*, 2022, **342**, 53–65.
4 A. M. Vargason, A. C. Anselmo and S. Mitragotri, The evolution of commercial drug delivery technologies, *Nat. Biomed. Eng.*, 2021, **5**, 951–967.
5 W. Fan, B. Yung, P. Huang and X. Chen, Nanotechnology for Multimodal Synergistic Cancer Therapy, *Chem. Rev.*, 2017, **117**, 13566–13638.
6 S. Park, A. Aalipour, O. Vermesh and J. H. Yu, Towards clinically translatable in vivo nanodiagnostics, *Nat. Rev. Mater.*, 2017, **2**, 17014.
7 J. Shi, P. W. Kantoff, R. Wooster and O. C. Farokhzad, Cancer nanomedicine: progress, challenges and opportunities, *Nat. Rev. Cancer*, 2017, **17**, 20–37.
8 B. A. Kairdolf, A. M. Smith, T. H. Stokes, M. D. Wang, A. N. Young and S. M. Nie, Semiconductor Quantum Dots for Bioimaging and Biodiagnostic Applications, *Annu. Rev. Anal. Chem.*, 2013, **6**, 143–162.
9 C. Tassa, S. Y. Shaw and R. Weissleder, Dextran-Coated Iron Oxide Nanoparticles: A Versatile Platform for Targeted

Molecular Imaging, Molecular Diagnostics, and Therapy, *Acc. Chem. Res.*, 2011, **44**, 842–852.
10 E. Phillips, O. Penate-Medina, P. B. Zanzonico, R. D. Carvajal, P. Mohan, Y. Ye, J. Humm, M. Gonen, H. Kalaigian, H. Schoder, H. M. Strauss, S. M. Larson, U. Wiesner and M. S. Bradbury, Clinical translation of an ultrasmall inorganic optical-PET imaging nanoparticle probe, *Sci. Trans. Med.*, 2014, **6**, 260ra149.
11 S. Friedrichs and D. M. Bowman, COVID-19 may become nanomedicine's finest hour yet, *Nat. Nanotechnol.*, 2021, **16**, 358–364.
12 Y. Barenholz, Doxil®—The first FDA-approved nano-drug: Lessons learned, *J. Controlled Release*, 2012, **160**, 117–134.
13 L. R. Brown, Commercial challenges of protein drug delivery, *Expert Opin. Drug Delivery*, 2005, **2**, 29–42.
14 M. Levin, *Pharmaceutical process scale-up*, Marcel Dekker, Inc., 2001.
15 Y. F. Maa and C. Hsu, Microencapsulation reactor scale-up by dimensional analysis, *J. Microencapsulation*, 1996, **13**, 53–66.
16 A. D. Bangham and R. W. Horne, Negative staining of phospholipids and their structural modification by surface-active agents as observed in the electron microscope, *J. Mol. Biol.*, 1964, **8**, 660–668.
17 U. Bulbake, S. Doppalapudi, N. Kommineni and W. Khan, Liposomal formulations in clinical use: an updated review, *Pharmaceutics*, 2017, **9**, 12.
18 A. Atinc, M. A. Maier, M. Manoharan, K. Fitzgerald, M. Jayaraman, S. Barros, S. Ansell, X. Du, M. J. Hope, T. D. Madden, B. L. Mui, S. C. Semple, Y. K. Tam, M. Ciufolini, D. Witzigmann, J. A. Kulkarni, R. van der Meel and P. R. Cullis, The Onpattro story and the clinical translation of nanomedicines containing nucleic acid-based drugs, *Nat. Nanotechnol.*, 2019, **14**, 1084–1087.
19 S. Friedrichs and D. M. Bowman, COVID-19 may become nanomedicine's finest hour yet, *Nat. Nanotechnol.*, 2021, **16**, 362–364.
20 S. Shahh, V. Dhawan, R. Holm, M. S. Nagarsenker and Y. Perrie, Liposomes: Advancements and innovation in the manufacturing process, *Adv. Drug Delivery Rev.*, 2020, **14**, 102–122.
21 A. Wagner, K. Vorauer-Uhl and K. H. Katinger, Liposomes produced in a pilot scale: production, purification and efficiency aspects, *Eur. J. Pharm. Biopharm.*, 2002, **54**, 213–219.
22 O. R. Justo and A. M. Moraes, Economical feasibility evaluation of an ethanol injection liposome production plant, *Chem. Eng. Technol.*, 2010, **33**, 15–20.
23 A. Wagner, K. Vorauer-Uhl, G. Kreismayr and H. Katinger, The crossflow injection technique: an improvement of the ethanol injection method, *J. Liposome Res.*, 2002, **12**, 259–270.
24 A. Wagner, K. Vorauer-Uhl, G. Kreismayr and H. Katinger, Enhanced protein loading into liposomes by the multiple crossflow injection technique, *J. Liposome Res.*, 2002, **12**, 271–283.
25 T. T. Pham, C. Jaafar-Maalej, C. Charcosset and H. Fessi, Liposome and niosome preparation using a membrane contactor for scale-up, *Colloids Surf., B*, 2012, **94**, 15–21.
26 Y. Liu, G. Z. Yang, Y. Hui, S. Ranaweera and C. X. Zhao, Microfluidic nanoparticles for drug delivery, *Small*, 2022, **18**, 2106580.
27 R. C. Xu, M. A. Tomeh, S. Y. Ye, P. Zhang, S. W. Lv, R. R. You, N. Wang and X. B. Zhao, Novel microfluidic swirl mixers for scalable formulation of curcumin loaded liposomes for cancer therapy, *Int. J. Pharm.*, 2022, **622**, 121857.
28 A. Yaghmur, A. Ghazal, R. Ghazal, M. Dimaki and W. E. Svendsen, A hydrodynamic flow focusing microfluidic device for the continuous production of hexosomes based on docosahexaenoic acid monoglyceride, *Phys. Chem. Chem. Phys.*, 2019, **21**, 13005–13013.
29 C. X. Zhao, L. He, S. Z. Qiao and A. P. Middelberg, Nanoparticle synthesis in microreactors, *Chem. Eng. Sci.*, 2011, **66**, 1463–1479.
30 S. Marre and K. F. Jensen, Synthesis of micro and nanostructures in microfluidic systems, *Chem. Soc. Rev.*, 2010, **39**, 1183–1202.
31 A. Sealy Manufacturing moonshot: How Pfizer makes its millions of Covid-19 vaccine doses. **https://edition.cnn.com/2021/03/31/health/pfizer-vaccine-manufacturing/index.html**.
32 H. Zhang, J. Yang, R. Sun, S. Han, Z. Yang and L. Teng, Microfluidics for nano-drug delivery systems: from fundamentals to industrialization, *Acta Pharm. Sin. B*, 2023, DOI: **10.1016/j.apsb.2023.01.018**.
33 M. Lu, A. Ozcelik, C. L. Grigsby, Y. Zhao, F. Guo, K. W. Leong and T. J. Huang, Microfluidic hydrodynamic focusing for synthesis of nanomaterials, *Nano Today*, 2016, **11**, 778–792.
34 N. Kamaly, G. Fredman, J. J. R. Fojas, M. Subramanian, W. I. Choi, K. Zepeda, C. Vilos, M. Y. Yu, S. Gadde, J. Wu, J. Milton, R. C. Leitao, L. R. Fernandes, M. Hasan, H. Y. Gao, V. Nguyen, J. Harris, I. Tabas and O. C. Farokhzad, Targeted interleukin-10 nanotherapeutics developed with a microfluidic chip enhance resolution of inflammation in advanced atherosclerosis, *ACS Nano*, 2016, **10**, 5280–5292.
35 H. Cho, J. Kim, K. Suga, T. Ishigami, H. Park, J. W. Bang, S. Seo, M. Choi, P. S. Chang, H. Umakoshi, S. Jung and K. Y. Suh, Microfluidic platforms with monolithically integrated hierarchical apertures for the facile and rapid formation of cargo-carrying vesicles, *Lab Chip*, 2015, **15**, 373–377.
36 A. D. Stroock, S. K. Dertinger, A. Ajdari, I. Mezic, H. A. Stone and G. M. Whitesides, Chaotic mixer for microchannels, *Science*, 2002, **295**, 647–651.
37 E. Kastner, R. Kaur, D. Lowry, B. Moghaddam, A. Wilkinson and Y. Perrie, High-throughput manufacturing of size-tuned liposomes by a new microfluidics method using enhanced statistical tools for characterization, *Int. J. Pharm.*, 2014, **477**, 361–368.
38 C. C. L. Cheung and W. T. Al-Jamal, Sterically stabilized liposomes production using staggered herringbone

micromixer: Effect of lipid composition and PEG-lipid content, *Int. J. Pharm.*, 2019, **566**, 687–696.

39 P. H. Huang, S. Zhao, H. Bachman, N. Nanna, Z. Li, C. Chen, S. Yang, M. Wu, S. P. Zhang and T. J. Huang, Acoustofluidics nanomaterial synthesis: acoustofluidic synthesis of particulate nanomaterials, *Adv. Sci.*, 2019, **6**, 1970113.

40 N. H. A. Le, H. Deng, C. Devendran, N. Akhtar, X. Ma, C. Pouton, H. K. Chan, A. Neild and T. Alan, Ultrafast star-shaped acoustic micromixer for high throughput nanoparticle synthesis, *Lab Chip*, 2020, **20**, 582–591.

41 C. Walsh; K. Ou; N. M. Belliveau; T. J. Leaver; A. W. Wild; J. Huft; P. J. Lin; S. Chen; A. K. Leung and J. B. Lee, in *Drug Delivery System*, ed. Jain K. K., Springer, Berlin, 2014, 109–120.

42 Z. Dong, Z. Wen, Z. Fang, S. Kuhn and T. Noel, Scale-up of micro- and milli-reactors: an overview of strategies, design principles and applications, *Chem. Eng. Sci.: X*, 2021, **10**, 100097.

43 L. R. Brown, Commercial challenges of protein drug delivery, *Expert Opin. Drug Delivery*, 2005, **2**, 29–42.

44 K. Park, S. Skidmore, J. Hadar, J. Garner, H. Park, A. Otte, B. K. Soh, G. Yoon, D. Yu, Y. Yun, B. K. Lee, X. J. Jiang and Y. Wang, Injectable, long-acting PLGA formulations: analyzing PLGA and understanding microparticle formation, *J. Controlled Release*, 2019, **304**, 125–134.

45 K. Park, A. Otte, F. Sharifi, J. Garner, S. Skidmore, H. Park, Y. K. Jhon, B. Qin and Y. Wang, Formulation composition, manufacturing process, and characterization of poly(lactide-*co*-glycolide) microparticles, *J. Controlled Release*, 2021, **329**, 1150–1161.

46 J. Zhou, K. Hirotta, R. Ackermann, J. Walker, Y. Wang, S. Choi, A. Schwendeman and S. P. Schwendeman, Reverse engineering the 1-month Lupron depot®, *AAPS J.*, 2018, **20**, 105.

47 S. D. Allison, Effect of structural relaxation on the preparation and drug release behavior of PLGA microparticle drug delivery system, *J. Pharm. Sci.*, 2007, **97**, 2022–2035.

48 J. Vysloužil, J. P. Doležel, M. Kejdusova, E. Mašková, J. Mašek, R. Lukáč, V. Kostal, D. Vetchy and K. K. Dvorackova, Influence of different formulations and process parameters during the preparation of drug-loaded PLGA microspheres evaluated by multivariate data analysis, *Acta Pharma.*, 2014, **64**, 403–417.

49 K. Elkharraz, N. Faisant, C. Guse, F. Siepmann, B. Arica-Yegin, J. M. Oger, R. Gust, A. Goepferich, J. P. Benoit and J. Siepmann, Paclitaxel-loaded microparticles and implants for the treatment of brain cancer: preparation and physicochemical characterization, *Int. J. Pharm.*, 2006, **314**, 127–136.

50 C. Martin-Sabroso, A. I. Fraguas-Sanchez, J. Aparicio-Blanco, M. F. Cano-Abad and A. I. Torres-Suarez, Critical attributes of formulation and of elaboration process of PLGA-protein microparticles, *Int. J. Pharm.*, 2015, **480**, 27–36.

51 K. Vay, W. Frieß and S. Scheler, A detailed view of microparticle formation by in-process monitoring of the glass transition temperature, *Eur. J. Pharm. Biopharm.*, 2012, **81**, 399–408.

52 J. V. Andhariya, J. Shen, Y. Wang, S. Choi and D. J. Burgess, Effect of minor manufacturing changes on stability of compositionally equivalent PLGA microspheres, *Int. J. Pharm.*, 2019, **566**, 532–540.

53 Z. Q. Liu, X. Li, B. S. Xiu, C. M. Duan, J. X. Li, X. H. Zhang, X. Q. Yang, W. H. Dai, H. Johnson, H. Q. Zhang and X. Y. Feng, A novel and simple preparative method for uniform-sized PLGA microspheres: Preliminary application in antitubercular drug delivery, *Colloids Surf., B*, 2016, **145**, 679–687.

54 F. Sharifia, A. Ottea, G. Yoona and K. Park, Continuous in-line homogenization process for scale-up production of naltrexone-loaded PLGA microparticles, *J. Controlled Release*, 2020, **325**, 347–358.

55 W. S. Saad and R. K. Prud'homme, Principles of nanoparticle formation by flash nanoprecipitation, *Nano Today*, 2016, **11**, 212–227.

56 B. K. Johnson and R. K. Prud'homme, Chemical processing and micromixing in confined impinging jets, *AIChE J.*, 2003, **49**, 2264–2282.

57 H. Z. Hu, C. Yang, M. Q. Li, D. Shao, H. Q. Mao and K. W. Leong, Flash technology-based self-assembly in nanoformulation: fabrication to biomedical applications, *Mater. Today*, 2021, **42**, 99–116.

58 Y. Liu, C. Cheng, Y. Liu, R. K. Prud'homme and R. Fox, Mixing in a multi-inlet vortex mixer (MIVM) for flash nanoprecipitation, *Chem. Eng. Sci.*, 2008, **63**, 2829–2842.

59 J. C. Cheng, M. G. Olsen and R. Fox, A microscale multi-inlet vortex nanoprecipitation reactor: Turbulence measurement and simulation, *Appl. Phys. Lett.*, 2009, **94**, 204104.

60 L. Le, A. Bokare and F. Erogbogbo, Hand powered, cost effective, 3D printed nanoparticle synthesizer: effects of polymer end caps, drugs, and solvents on lipid polymer hybrid nanoparticles, *Mater. Res. Express*, 2019, **6**, 025403.

61 M. Icardi, E. Gavi, D. L. Marchisioa, A. A. Barresi, M. G. Olsenc, R. O. Fox and D. Lakeha, Investigation of the flow field in a three-dimensional Confined Impinging Jets Reactor by means of microPIV and DNS, *Chem. Eng. J.*, 2011, **166**, 294–305.

62 J. C. Cheng and R. O. Fox, Kinetic modeling of nanoprecipitation using CFD coupled with a population balance, *Ind. Eng. Chem. Res.*, 2010, **49**, 10651.

63 N. Di Pasquale, D. L. Marchisio and A. A. Barresi, Model validation for precipitation in solvent-displacement processes, *Chem. Eng. Sci.*, 2012, **84**, 671–683.

64 A. Nikoubashman, V. E. Lee, C. Sosa, R. K. Prud'homme, R. D. Priestley and A. Z. Panagiotopoulos, Directed assembly of soft colloids through rapid solvent exchange, *ACS Nano*, 2016, **10**, 1425–1433.

65 D. L. Marchisio, Large eddy simulation of mixing and reaction in a confined impinging jets reactor, *Comput. Chem. Eng.*, 2009, **33**, 408–420.

66 E. Gavi, D. L. Marchisio and A. A. Barresi, CFD modelling and scale-up of Confined Impinging Jet Reactors, *Chem. Eng. Sci.*, 2007, **62**, 2228–2241.

67 R. K. Prud'homme, W. Saad and L. Mayer, Paclitaxel conjugate block copolymer nanoparticle formation by flash nanoprecipitation, *NSTI Nanotech 2006, NSTI Nanotechnol. Conf. Trade Show*, 2006, **2**, 824–826.

68 K. M. Pustulka, A. R. Wohl, H. S. Lee, A. R. Michel, J. Han, T. R. Hoye, A. V. McComick, J. Panyam and C. W. Macosko, Flash nanoprecipitation: particle structure and stability, *Mol. Pharmaceutics*, 2013, **10**, 4367–4377.

69 Y. T. Tam, K. K. W. To and A. H. L. Chow, Fabrication of doxorubicin nanoparticles by controlled antisolvent precipitation for enhanced intracellular delivery, *Colloids Surf., B*, 2016, **139**, 249–258.

70 E. Tripodi, A. Lazidis, I. T. Norton and F. Spyropoulos, Production of oil-in-water emulsions with varying dispersed-phase content using confined impinging jet mixers, *Ind. Eng. Chem. Res.*, 2019, **58**, 14859–14872.

71 Y. Z. Hu, Y. N. Zhu, N. D. Sutherland, D. R. Wilson, M. Pang, E. E. Liu, J. R. Staub, C. A. Berlinicke, D. J. Zack, J. J. Green, S. K. Reddy and H. Q. Mao, Size-controlled and shelf-stable DNA particles for production of lentiviral vectors, *Nano Lett.*, 2021, **21**, 5697–5705.

72 G. Bovone, E. A. Guzzi and M. W. Tibbitt, Flow-based reactor design for the continuous production of polymeric nanoparticles, *AIChE J.*, 2019, **65**, e16840.

73 Z. He, Z. Liu, H. Tian, Y. Hu, L. Liu, K. W. Leong, H. Q. Mao and Y. Chen, Scalable production of core–shell nanoparticles by flash nanocomplexation to enhance mucosal transport for oral delivery of insulin, *Nanoscale*, 2018, **10**, 3307.

74 Z. Zeng, C. Dong, P. Zhao, Z. Liu, L. Liu, H. Q. Mao, K. W. Leong, X. Gao and Y. Chen, Scalable production of therapeutic protein nanoparticles using flash nanoprecipitation, *Adv. Healthcare Mater.*, 2019, **8**, 1801010.

75 H. Hu, C. Yang, F. Zhang, M. Li, Z. Tu, L. Mu, J. Dawulieti, Y. H. Lao, Z. Xiao, H. Yan, W. Sun, D. Shao and K. W. Leong, A versatile and robust platform for the scalable manufacture of biomimetic nanovaccines, *Adv. Sci.*, 2021, **8**, 2002020.

76 Y. Shamay, J. Shah, M. Isik, A. Mizrachi, J. Leibold, D. F. Tschaharganeh, D. Roxbury, J. Budhathoki-Uprety, K. Nawaly, J. L. Sugarman, E. Baut, M. R. Neiman, M. Dacek, K. S. Ganesh, D. C. Johnson, R. Sridharan, K. L. Chu, V. K. Rajasekhar, S. W. Lowe, J. D. Chodera and D. A. Heller, *Nat. Mat.*, 2018, **17**, 361–368.

77 B. K. Johnson and R. K. Prud'homme, Flash nanoprecipitation of organic actives and block copolymers using a confined impinging jets ixer, *Aust. J. Chem.*, 2003, **56**, 1021–1024.

78 H. Shen, S. Hong, R. K. Prud'Homme and Y. Liu, Self-assembling process of flash nanoprecipitation in a multi-inlet vortex mixer to produce drug-loaded polymeric nanoparticles, *J. Nanopart. Res.*, 2011, **13**, 4109–4120.

79 B. K. Johnson and R. K. Prud'homme, Mechanism for rapid self-assembly of block copolymer nanoparticles, *Phys. Rev. Lett.*, 2003, **91**, 118302.

80 E. Hoogenboezem and C. L. Duvall, Harnessing albumin as a carrier for cancer therapies, *Adv. Drug Delivery Rev.*, 2018, **130**, 73–89.

81 K. Langer, S. Balthasar, V. Vogel, N. Dinauer, H. von Briesen and D. Schubert, Optimization of the preparation process for human serum albumin (HSA) nanoparticles, *Int. J. Pharm.*, 2003, **257**, 169–180.

82 M. Wacker, A. Zensi, J. Kufleitner, A. Ruff, J. Schutz, T. Stockburger, T. Marstaller and V. Vogel, A toolbox for the upscaling of ethanolic human serum albumin (HSA) desolvation, *Int. J. Pharm.*, 2011, **414**, 225–232.

83 L. Gopakumar, M. Sreeranganathan, S. Chappan, S. James, G. S. Gowd, M. Manohar, A. Sukumaran, A. K. K. Unni, S. V. Nair and M. Koyakutty, Enhanced oral bioavailability and antitumor therapeutic efficacy of sorafenib administered in core-shell protein nanoparticle, *Drug Delivery Transl. Res.*, 2022, **12**, 2824–2837.

84 N. Desai, V. Trieu, Z. W. Yao, L. Louie, S. Ci, A. Yang, C. L. Tao, T. De, B. Beals, D. Dykes, P. Noker, R. Yao, E. Labao, M. Hawkins and P. Soon-Shiong, Increased antitumor activity, intratumor paclitaxel concentrations, and endothelial cell transport of cremophor-free, albumin-bound paclitaxel, ABI-007, compared with cremophor-based paclitaxel, *Clin. Cancer Res.*, 2006, **12**, 1317–1324.

85 R. Li, T. S. C. Ng, S. J. Wang, M. Prytyskach, C. B. Rodel, H. Mikula, R. H. Kohler, M. A. Garlin, D. A. Lauffenburger, S. Parangi, D. M. Dinulescu, N. Bardeesy, R. Weissleder and M. A. Miller, Therapeutically reprogrammed nutrient signaling enhances nanoparticulate albumin bound drug uptake and efficacy in KRAS-mutant cancer, *Nat. Nanotechnol.*, 2021, **16**, 830–839.

86 B. Elsadek and F. Kratz, Impact of albumin on drug delivery—new applications on the horizon, *J. Controlled Release*, 2012, **157**, 4–28.

87 P. Nimbalkar, P. Tabada, A. Bokare, J. Chung, M. Mousavi, M. Simon and F. Erogbogbo, Improving the physiological relevance of drug testing for drug-loaded nanoparticles using 3D tumor cell cultures, *MRS Commun.*, 2019, **9**, 1053–1059.

88 R. H. Fang, K. N. H. Chen, S. Aryal, C. M. J. Hu, K. Zhang and L. F. Zhang, Large-scale synthesis of lipid-polymer hybrid nanoparticles using a multi-inlet vortex reactor, *Langmuir*, 2012, **28**, 13824–13829.

89 J. Wen, K. Yang, F. Y. Liu, H. J. Li, Y. Q. Xu and S. G. Sun, Diverse gatekeepers for mesoporous silica nanoparticle based drug delivery systems, *Chem. Soc. Rev.*, 2017, **46**, 6024–6045.

90 R. K. Kankala, Y. H. Han, J. Na, C. H. Lee, Z. Sun, S. B. Wang, T. Kimura, Y. S. Ok, Y. Yamauchi and A. Z. Chen, Nanoarchitectured structure and surface biofunctionality of mesoporous silica nanoparticles, *Adv. Mater.*, 2020, **32**, e1907035.

91 G. Yang, Y. Liu, H. Wang, R. Wilson, Y. Hui, L. Yu, D. Wibowo, C. Zhang, A. K. Whittaker and A. P. Middelberg, Bioinspired core-shell nanoparticles for hydrophobic drug delivery, *Angew. Chem., Int. Ed.*, 2019, **58**, 14357–14364.

92 W. Stober, A. Fink and E. Bohn, Controlled growth of monodisperse silica spheres in micron size range, *J. Colloid Interface Sci.*, 1968, **26**, 62–69.

93 C. Kim, S. Yoon and J. H. Lee, Facile large scale synthesis of mesoporous silica nanoparticles at room temperature in a monophasic system with fine size control, *Microporous Mesoporous Mater.*, 2019, **288**, 109595.
94 Z. Fu, L. Li, Y. Wang, Q. Chen, F. Zhao, L. Dai, Z. Chen, D. Liu and X. Guo, Direct preparation of drug-loaded mesoporous silica nanoparticles by sequential flash nanoprecipitation, *Chem. Eng. J.*, 2020, **382**, 122905.
95 S. Pal, K. Madane and A. A. Kulkarni, Antisolvent based precipitation: Batch, capillary flow reactor and impinging jet reactor, *Chem. Eng. J.*, 2019, **369**, 1161–1171.
96 C. B. Gao, F. L. Lyu and Y. D. Yin, Encapsulated metal nanoparticles for catalysis, *Chem. Rev.*, 2021, **121**, 834–881.
97 S. M. Dizai, F. Lotfipour, M. Barzegar-Jalali, M. Zarrintan and K. Adibkia, Antimicrobial activity of the metals and metal oxide nanoparticles, *Mater. Sci. Eng., C*, 2014, **44**, 278–284.
98 J. B. Deshpande and A. A. Kulkarni, Reaction engineering for continuous production of silver nanoparticles, *Chem. Eng. Technol.*, 2018, **41**, 157–167.
99 J. Wagner, T. Kirner, G. Mayer, J. Albert and J. M. Köhler, Generation of metal nanoparticles in a microchannel reactor, *Chem. Eng. J.*, 2004, **101**, 251.
100 J. Wagner, T. R. Tshikhudo and J. M. Köhler, Microfluidic generation of metal nanoparticles by borohydride reduction, *Chem. Eng. J.*, 2008, **135**, S104.
101 R. Baber, L. Mazzei, N. T. K. Thanh and A. Gavriilidis, Synthesis of silver nanoparticles in a microfluidic coaxial flow reactor, *RSC Adv.*, 2015, **5**, 95585.
102 A. Knauer, A. Eisenhardt, S. Krischok and J. M. Koehler, Nanometer precise adjustment of the silver shell thickness during automated Au–Ag core–shell nanoparticle synthesis in micro fluid segment sequences, *Nanoscale*, 2014, **6**, 5230.
103 J. M. Köhler, H. Romanus, U. Hübner and J. Wagner, Formation of star-like and core-shell Au Ag nanoparticles during two- and three-step preparation in batch and in microfluidic systems, *J. Nanomater.*, 2007, **2007**, 098134.
104 L. Xu, J. Peng, C. Srinivasakannan, L. Zhang, D. Zhang, C. Liu, S. Wang and A. Q. Shen, Synthesis of copper nanoparticles by a T-shaped microfluidic device, *RSC Adv.*, 2014, **4**, 25155.
105 A. Pekkari, Z. Say, A. Susarrey-Arce, C. Langhammer, H. Härelind, V. Sebastian and K. Moth-Poulsen, Continuous microfluidic synthesis of Pd nanocubes and PdPt core−shell nanoparticles and their catalysis of NO_2 reduction, *ACS Appl. Mater. Interfaces*, 2019, **11**, 36196.
106 X. Li, Q. Feng and X. Jiang, Microfluidic synthesis of Gd-based nanoparticles for fast and ultralong MRI signals in the solid tumor, *Adv. Healthcare Mater.*, 2019, **8**, 1900672.
107 S. Y. Tang, R. Qiao, S. Yan, D. Yuan, Q. Zhao, G. Yun, T. P. Davis and W. Li, Microfluidic mass production of stabilized and stealthy liquid metal nanoparticles, *Small*, 2018, **14**, 1800118.
108 A. K. Hauser, R. J. Wydra, N. A. Stocke, K. W. Anderson and J. Z. Hilt, Magnetic nanoparticles and nanocomposites for remote controlled therapies, *J. Controlled Release*, 2015, **219**, 76–94.
109 T. H. Shin, Y. Choi, S. Kima and J. Cheon, Recent advances in magnetic nanoparticle-based multi-modal imaging, *Chem. Soc. Rev.*, 2015, **44**, 4501–4516.
110 S. H. Noh, S. H. Moon, T. H. Shin, Y. Lim and J. Cheon, Recent advances of magneto-thermal capabilities of nanoparticles: from design principles to biomedical applications, *Nano Today*, 2017, **13**, 61–76.
111 A. Ali, T. Shah, R. Ullah, P. Zhou, M. Guo, M. Ovis, Z. Tan and Y. Rui, Review on recent progress in magnetic nanoparticles: synthesis, characterization, and diverse applications, *Front. Chem.*, 2021, **9**, 629054.
112 Z. Li, B. Tan, M. Allix, A. I. Cooper and M. J. Rosseinsky, Direct coprecipitation route to monodisperse dual-functionalized magnetic iron oxide nanocrystals without size selection, *Small*, 2008, **4**, 231–239.
113 L. Panariello, G. Wu, M. O. Besenhard, K. Loizou, L. Storozhuk, N. T. K. Thanh and A. Gavriilidis, A modular millifluidic platform for the synthesis of iron oxide nanoparticles with control over dissolved gas and flow configuration, *Materials*, 2020, **13**, 1019.
114 A. Larrea, V. Sebastian, A. Ibarra, M. Arruebo and J. Santamaria, Gas slug microfluidics: a unique tool for ultrafast, highly controlled growth of iron oxide nanostructures, *Chem. Mater.*, 2015, **27**, 4254–4260.
115 K. Kumar, A. M. Nightingale, S. H. Krishnadasan, N. Kamaly, M. Wylenzinska-Arridge, K. Zeissler, W. R. Branford, E. Ware, A. J. deMello and J. C. deMello, Direct synthesis of dextran-coated superparamagnetic iron oxide nanoparticles in a capillary-based droplet reactor, *J. Mater. Chem.*, 2012, **22**, 4704–4708.
116 N. Deng, Y. Wang and G. Luo, A novel method for fast and continuous preparation of superfine titanium dioxide nanoparticles in microfluidic system, *Particuology*, 2022, **60**, 61–67.
117 P. Stolzenburg, T. Lorenz, A. Dietzel and G. Garnweitner, Microfluidic synthesis of metal oxide nanoparticles via the nonaqueous method, *Chem. Eng. Sci.*, 2018, **191**, 500–510.
118 B. A. Kairdolf, A. M. Smit, T. H. Stokes, M. D. Wang, A. N. Young and S. Nie, Semiconductor quantum dots for bioimaging and biodiagnostic applications, *Annu. Rev. Anal. Chem.*, 2013, **6**, 143–162.
119 C. B. Murray, C. R. Kagan and M. G. Bawendi, Synthesis and characterization of monodisperse nanocrystals and close-packed nanocrystal assemblies, *Annu. Rev. Mater. Sci.*, 2000, **30**, 545–610.
120 J. Li, Y. A. Wang, W. Guo, J. C. Keay, T. D. Mishima, M. B. Johnson and X. Peng, Large-scale synthesis of nearly monodisperse CdSe/CdS core/shell nanocrystals using air-stable reagents via successive ion layer adsorption and reaction, *J. Am. Chem. Soc.*, 2003, **125**, 12567–12575.
121 W. Zhang, H. Zhang, Y. Feng and X. Zhong, Scalable single-step noninjection synthesis of high-quality core/shell quantum dots with emission tunable from violet to near infrared, *ACS Nano*, 2012, **6**, 11066–11073.
122 J. Edel, R. Fortt, J. C. deMello and A. J. deMello, Microfluidics routes to the controlled production of nanoparticles, *Chem. Commun.*, 2002, 1136–1137.

123 E. M. Chan, R. A. Mathies and A. P. Alivisatos, Size-controlled growth of CdSe nanocrystals in microfluidic reactors, *Nano Lett.*, 2003, **3**, 199–201.
124 E. M. Chan, A. P. Alivisatos and R. A. Mathies, High-temperature microfluidic synthesis of CdSe nanocrystals in nanoliter droplets, *J. Am. Chem. Soc.*, 2005, **127**, 13854–13861.
125 G. X. Li, Q. Li, R. Cheng and S. Chen, Synthesis of quantum dots based on microfluidic technology, *Curr. Opin. Chem. Eng.*, 2020, **29**, 34–41.
126 A. D. Duong, G. Ruan, K. Mahajan, J. O. Winter and B. E. Wyslouzil, Scalable, Semicontinuous production of micelles encapsulating nanoparticles via electrospray, *Langmuir*, 2014, **30**, 3939–3948.
127 K. H. Lee, G. L. Z. Yang, B. E. Wyslouzil and J. O. Winter, Electrohydrodynamic mixing-mediated nanoprecipitation for polymer nanoparticle synthesis, *ACS Appl. Polym. Mater.*, 2019, **1**, 691–700.
128 X. Y. Ding, N. Han, J. Wang, Y. X. Sun and G. Ruan, Effects of organic solvents on the structures of micellar nanocrystals, *RSC Adv.*, 2017, **7**, 16131–16138.
129 X. Y. Ding, Y. X. Sun, Y. M. Chen, W. C. Ding, S. Emory, T. H. Li, Z. X. Xu, N. Han, J. Wang and G. Ruan, Fabrication of spherical and worm-shaped micellar nanocrystals by combining electrospray, self-assembly, and solvent-based structure control, *J. Visualized Exp.*, 2018, **132**, e56657.
130 X. Yong, Y. M. Chen, X. Y. Yu and G. Ruan, Producing protein-nanoparticle co-assembly supraparticles by the interfacial instability process, *Soft Matt.*, 2019, **15**, 7420–7428.
131 J. R. Lloyd, J. M. Byrne and V. S. Coker, Biotechnological synthesis of functional nanomaterials, *Curr. Opin. Biotechnol*, 2011, **22**, 509–515.
132 A. M. Fayaz, K. Balaji, M. Girilal, R. Yadav, P. T. Kalaichelvan and R. Venketesan, Biogenic synthesis of silver nanoparticles and their synergistic effect with antibiotics: a study against Gram-positive and Gram-negative bacteria, *Nanomed. Nanotechnol.*, 2010, **6**, 103–109.
133 N. Law, S. Ansari, F. R. Livens, J. C. Renshaw and J. R. Lloyd, Formation of nanoscale elemental silver particles via enzymatic reduction by Geobacter sulfurreducens, *Appl. Environ. Microbiol.*, 2008, **74**, 7090–7093.
134 J. W. Moon, C. J. Rawn, A. J. Rondinone, L. J. Love, Y. Roh, S. M. Everett, R. J. Lauf and T. J. Phelps, Large-scale production of magnetic nanoparticles using bacterial fermentation, *J. Ind. Microbiol. Biotechnol.*, 2010, **37**, 1023–1031.
135 M. Hassanisaadi, G. H. S. Bonjar, A. Rahdar, S. Pandey, A. Hosseinipour and R. Abdolshahi, Environmentally safe biosynthesis of gold nanoparticles using plant water extracts, *Nanomaterials*, 2021, **11**, 2033.
136 H. F. Bao, Z. S. Lu, X. Q. Cui, Y. Qiao, J. Guo, J. M. Anderson and C. M. Li, Extracellular microbial synthesis of biocompatible CdTe quantum dots, *Acta Biomater.*, 2010, **6**, 3534–3541.
137 F. Fang, M. Li, J. Zhang and C. S. Lee, Different strategies for organic nanoparticle preparation in biomedicine, *ACS Mater. Lett.*, 2020, **2**, 531–549.
138 R. Thiruvengadathan, V. Korampally, A. Ghosh, N. Chanda, K. Gangopadhyay and S. Gangopadhyay, Nanomaterial processing using self-assembly-bottom-up chemical and biological approaches, *Rep. Prog. Phys.*, 2013, **76**, 066501.
139 Z. M. Sherman and J. W. Swan, Dynamic, directed self-assembly of nanoparticles via toggled interactions, *ACS Nano*, 2016, **10**, 5260–5271.
140 J. Feng, C. E. Markwalter, C. Tian, M. Armstrong and R. K. Prud'homme, Translational formulation of nanoparticle therapeutics from laboratory discovery to clinical scale, *J. Transl. Med.*, 2019, **17**, 200.
141 G. Cotin, B. Heinrich, F. Perton, C. Kiefer, G. Francius, D. Mertz, B. Freis, B. Pichon, J.-M. Strub, S. Cianferani, N. O. Pena, D. Ihiawakrim, D. Portehault, O. Ersen, A. Khammari, M. Picher, F. Banhart, C. Sanchez and S. Begin-Colin, A confinement-driven nucleation mechanism of metal oxide nanoparticles obtained via thermal decomposition in organic media, *Small*, 2022, **18**, e2200414.
142 S. Mozaffari, W. Li, M. Dixit, S. Seifert, B. Lee, L. Kovarik, G. Mpourmpakis and A. M. Karim, The role of nanoparticle size and ligand coverage in size focusing of colloidal metal nanoparticles, *Nanoscale Adv.*, 2019, **1**, 4052–4066.
143 M. C. Operti, A. Bernhardt, S. Grimm, A. Engel, C. G. Figdor and O. Tagit, PLGA-based nanomedicines manufacturing: Technologies overview and challenges in industrial scale-up, *Int. J. Pharm.*, 2021, **605**, 120807.
144 H. W. Liu, Y. Z. Hu, Y. Ren, H. Nam, J. L. Santos, S. Ng, L. K. Gong, M. Brummet, C. A. Carrington, C. G. Ullman, M. G. Pomper, I. Minn and H. Q. Mao, Scalable purification of plasmid DNA nanoparticles by tangential flow filtration for systemic delivery, *ACS Appl. Mater. Interfaces*, 2021, **13**, 30326–30336.
145 E. V. Semenov, A. A. Slavyanskiy and D. P. Mitroshina, Numerical analysis of emulsion separation processes in a continuous centrifuge, *Chem. Pet. Eng.*, 2021, **57**, 113–121.
146 L. K. Shekhawat, J. Sarkar, R. Gupta, S. Hadpe and A. S. Rathore, Application of CFD in bioprocessing: separation of mammalian cells using disc stack centrifuge during production of biotherapeutics, *J. Biotechnol.*, 2018, **10**, 1–11.
147 P. M. Doran, *Bioprocess Engineering Principles*, 2nd edn, 2013.
148 A. Wicki, R. Ritschard, U. Loesch, S. Deuster, C. Rochlitz and C. Mamot, Large-scale manufacturing of GMP-compliant anti-EGFR targeted nanocarriers: production of doxorubicin-loaded anti-EGFR immunoliposomes for a first-in-human clinical trial, *Int. J. Pharm.*, 2015, **484**, 8–15.
149 R. M. F. van der Put, C. Smitsman, A. de Haan, M. Hamzink, H. Timmermans, J. Uittenbogaard, J. Westdijk, M. Stork, O. Ophorst, F. Thouron, C. Guerreiro, P. J. Sansonetti, A. Phalipon and L. A. Mulard, The first-in-human synthetic glycan-based conjugate vaccine candidate against shigella, *ACS Cent. Sci.*, 2022, **8**, 449–460.
150 A. Thomas, B. A. Teicher and R. Hassan, Antibody–drug conjugates for cancer therapy, *Lancet Oncol.*, 2016, **17**, 254–262.
151 A. Beck, L. Goetsch, C. Dumontet and N. Corvaia, Strategies and challenges for the next generation of antibody–drug conjugates, *Nat. Rev. Drug Discovery*, 2017, **16**, 315–337.

152 R. Dere, J. H. Yi, C. Lei, O. Saad, C. Huang, Y. H. Li, J. Baudys and S. Kaur, PK assays for antibody-drug conjugates: case study with ado-trastuzumab emtansine, *Bioanalysis*, 2013, **5**, 1025–1040.

153 A. G. Polson, W. Y. Ho and V. Ramakrishnan, Investigational antibody-drug conjugates for hematological malignancies, *Expert Opin. Invest. Drugs*, 2011, **20**, 75–85.

154 B. A. Kellogg, L. Garrett, Y. Kovtun, K. C. Lai, B. Leece, M. Miller, G. Payne, R. Steeves, K. R. Whiteman and W. Widdison, Disulfide-linked antibody maytansinoid conjugates: optimization of in vivo activity by varying the steric hindrance at carbon atoms adjacent to the disulfide linkage, *Bioconjugate Chem.*, 2011, **22**, 717–727.

155 P. Agrawal and C. R. Bertozzi, Site-specific antibody–drug conjugates: the nexus of bioorthogonal chemistry, protein engineering, and drug development, *Bioconjugate Chem.*, 2015, **26**, 176–192.

156 Y. Matsuda, C. Clancy, Z. Tawfiq, V. Robles and B. Mendelsohn, Good manufacturing practice strategy for antibody-drug conjugate synthesis using site-specific chemical conjugation: first-generation AJICAP, *ACS Omega*, 2019, **4**, 20564–20570.

157 H. Ragelle, F. Danhier, V. Preat and R. Langer, Nanoparticle-based drug delivery systems: a commercial and regulatory outlook as the field matures, *Exp. Opin. Drug Delivery*, 2017, **14**, 851–864.

158 S. Bozdag, K. Dillen, J. Vandervoort and A. Ludwig, The effect of freeze-dryiny with different cryoprotectants and gamma-irradiation sterilization on the characteristics of ciprofloxacin HCl-loaded poly(D,L-lactide-glycolide) nanoparticles, *J. Pharm. Pharmacol.*, 2005, **57**, 699–707.

159 M. Fernandez, E. Barcia and S. Negro, Effect of gamma-irradiation on biodegradable microspheres loaded with rasagiline mesylate, *J. Chil. Chem. Soc.*, 2016, **61**, 3177–3180.

160 H. Keles, A. Naylor, F. Clegg and C. Sammon, Investigation of factors influencing the hydrolytic degradation of single PLGA microparticles, *Polym. Degrad. Stab.*, 2015, **119**, 228–241.

161 A. P. Ranjan, A. Mukerjee, L. Helson and J. K. Vishwanatha, Scale up, optimization and stability analysis of Curcumin C3 complex-loaded nanoparticles for cancer therapy, *J. Nanobiotechnol.*, 2012, **10**, 38.

162 E. Barcia, V. Sandoval, A. Fernandez-Carballido and S. Negro, Flunarizine-loaded microparticles for the prophylaxis of migraine, *J. Drug Delivery Sci. Technol.*, 2020, **60**, 102012.

163 I. P. Kaur, V. Kakkar, P. K. Deol, M. Yadav, M. Singh and I. Sharma, Issues and concerns in nanotech product development and its commercialization, *J. Controlled Release*, 2014, **193**, 51–62.

164 M. J. de Jesus Valle, A. Alves, P. Coutinho, M. P. Ribeiro, C. Maderuelo and A. S. Navarro, Lyoprotective effects of mannitol and lactose compared to sucrose and trehalose: sildenafil citrate liposomes as a case study, *Pharmaceutics*, 2021, **13**, 1164.

165 M. B. Adali, A. A. Barresi, G. Boccardo and R. Pisano, Spray freeze-drying as a solution to continuous manufacturing of pharmaceutical products in bulk, *Processes*, 2020, **8**, 709.

166 P. J. Van Bockstal, L. De Meyer, J. Corver, C. Vervaet and T. De Beer, Noncontact infrared-mediated heat transfer during continuous freeze-drying of unit doses, *J. Pharm. Sci.*, 2017, **106**, 71–82.

167 P. J. Van Bockstal, S. T. F. C. Mortier, L. De Meyer, J. Corver, C. Vervaet, I. Nopens and T. De Beer, Mechanistic modelling of infrared mediated energy transfer during the primary drying step of a continuous freeze-drying process, *Eur. J. Pharm. Biopharm.*, 2017, **114**, 11–21.